

COUPLED MULTIELECTRODE ARRAY SYSTEMS AND SENSORS FOR REAL-TIME CORROSION MONITORING - A REVIEW

Lietai Yang and Narasi Sridhar

Southwest Research Institute®
6220 Culebra Road
San Antonio, Texas 78238

ABSTRACT

This paper presents a review of multielectrode array systems and sensors for electrochemical studies and corrosion monitoring. Uncoupled multielectrode arrays [also called wire beam electrodes (WBEs)] for corrosion studies were reported in 1991. Coupled multielectrode arrays were first reported in 1996 for studying the spatiotemporal electrochemical behavior and corrosion processes, and in 1997 for mapping localized corrosion. More recently, coupled multielectrode array sensors (CMASs) have been used for real-time measurement of localized corrosion rates. The various application examples for the CMAS probes, including quantitative localized corrosion monitoring in aqueous solutions, wet gases, oil/water mixtures, salt deposits, biodeposits, soil, concrete, and undercoatings were reviewed. Some of the limitations of the multielectrode array systems are discussed.

Keywords: Corrosion monitoring, sensor array, electrode array, multiple electrodes, corrosion sensor, corrosion probe, real-time sensor, multielectrode sensor, coupled electrodes, localized corrosion, crevice corrosion, pitting corrosion, coupled multielectrode, WBE, CMAS.

INTRODUCTION

A multielectrode system is an integrated device that has multiple electrodes. In this paper, a multielectrode system is called a coupled multielectrode system if the electrodes in it are connected together through an external circuit and these electrodes are essentially at the same potential. A multielectrode system is called a multielectrode array if the electrodes in it are spatially arranged in a regular pattern (e.g., 4×4, or 10×10 array). The coupled multielectrode systems were reported for corrosion detection in concrete nearly two decades ago, and for crevice corrosion measurements nearly 13 years ago. The concept of multielectrode arrays was first reported, in the uncoupled form, 15 years ago for corrosion studies. The first published coupled multielectrode array was used for studying the spatiotemporal electrochemical behaviors and corrosion processes of iron in sulfuric acid solutions 10 years ago. Because the electrodes in a multielectrode array can be arranged in any given pattern and

each of electrodes is addressable, the coupled multielectrode arrays have been widely used by researchers to study the corrosion processes, especially the localized corrosion processes, of metals.

Recently, coupled multielectrode arrays have been used as sensors [called coupled multielectrode array sensors (CMASs)] for online and real-time monitoring of corrosion in laboratories and industrial fields. Because a CMAS does not require the presence of bulk electrolytes, CMAS probes have been used to quantitatively measure the localized corrosion of metals not only in aqueous solutions, but also in wet gases, oil/water mixtures, salt deposits, biodeposits, soil, concrete, and undercoatings. CMAS probes were also used for real-time monitoring of the performance of cathodic protection systems. In addition to the real-time measurement of the quantitative rate of localized corrosion, such as pitting and crevice corrosion, CMAS probes have also been used to measure the average corrosion rates. This paper presents a summary of the development of the coupled multielectrode array systems, with a focus on the applications of CMASs in laboratories and industrial fields. Some of the limitations of the coupled multielectrode array systems are also reviewed.

COUPLED MULTIELECTRODE SYSTEMS FOR CORROSION DETECTIONS

One of the devices described by Schiessl in a U.S. patent¹ issued in 1991, and in a patent application² initially filed in Germany in 1988 appeared to be the first coupled multielectrode system for corrosion monitoring (Figure 1). This coupled multielectrode system consisted of multiple steel anodes that were composed of materials similar to the reinforcement material and a corrosion-resistance cathode. Both the anodes and the cathode were embedded in a concrete structure. The steel anodes were spaced from one another at different distances from the external surface of the concrete structure, and each electrode was independently connected (coupled) to the cathode through a resistor. The coupling current from each anode to the cathode as a result of corrosion was measured by a voltage-measuring system that was connected to both ends of the resistor to establish the temporal course of the penetration of substances (e.g., chloride) that were capable of damaging the reinforcement. Similar applications in concrete were reported later in other publications by Schiessl and coworkers and by other investigators.³⁻⁸

In 1993, Steinsmo and coworkers reported on similar galvanically coupled multielectrode systems used to study the crevice corrosion of stainless steel materials in seawater.⁹⁻¹² Figure 2 shows the galvanically coupled multielectrode system used by Steinsmo and coworkers. In this system, several creviced stainless steel specimens were independently coupled to a large non-creviced specimen (similar to the creviced specimens in composition) through resistors. The corrosion process taking place in the crevices made the electrode potential of the creviced specimen more negative (or anodic) than the large non-creviced specimen (cathode) and produced a coupling current from the large non-creviced specimen to the creviced specimen. The coupling current was measured across its associated resistor and used to indicate the degree of crevice corrosion. The reference electrode in Figure 2 was used to measure the potential of the coupled multielectrode system.

Figure 3 shows typical results obtained with the coupled multielectrode system by Steinsmo, et al.¹¹ The measurement was conducted in a seawater test loop at 15°C, a condition the specimen is normally not subject to crevice corrosion. The purpose of this measurement was to study the effect of temporary upset conditions on crevice corrosion of a welded UNS S31254 material in seawater. Prior to the start of the measurement in Figure 3, the crevice specimens were temporarily aged at high temperatures and high electrochemical potentials to initiate crevice corrosion. Figure 3 shows that the corrosion attack continued to propagate at 15°C for 10 to 20 days before repassivation took place.

The multielectrode technique shown in Figures 1 and 2 requires only straightforward voltage measurements and yet is capable of detecting the onset of general and localized corrosion under service conditions. Depending on its accuracy and resolution, the voltage-monitoring instrument may be able to detect corrosion in the early stages of degradation. The disadvantage of this technique is that it cannot be used to determine the true rate of general or localized corrosion because of the large surface area of the crevice (5.5 cm^2 in Figure 2).

UNCOUPLED MULTIELECTRODE ARRAYS FOR CORROSION STUDIES

The first published uncoupled multielectrode array for corrosion studies [also called wire beam electrode WBE)] appears to be the one described by Tan and Tan, et al. in 1991 for measuring the corrosion behavior of carbon steel under oil-based coatings.¹³⁻¹⁴ Later, similar multielectrode arrays were used to study nonuniform corrosion under protective coatings and salt deposits.¹⁵⁻²¹ In a typical uncoupled multielectrode array, a large number of wires (0.5 to 2 mm in diameter) are flush-mounted in epoxy and arranged in a square configuration with the cross section exposed to an electrolyte. The spatial behavior of corrosion or the electrochemical heterogeneity is characterized by the measurement of the open-circuit potential map from each electrode, and by the measurement of the current map or electrical resistance map between pairs of selected wires.

COUPLED MULTIELECTRODE ARRAYS FOR SPATIOTEMPORAL CORROSION AND ELECTROCHEMICAL STUDIES

The first published coupled multielectrode array for corrosion and electrochemical studies appears to be the one described by Fei, et al. in 1996.²² The coupled multielectrode array was used to simulate a one-piece metal electrode for the study of the spatiotemporal electrochemical behavior of iron metal in a sulfuric acid solution. The electrode arrays consisted of 16 (a 2×8 rectangle or a 4×4 square) or 61 (a 5×5 hexagon) electrodes (cross section of 0.5-mm wires) embedded in epoxy (Figure 4).²²⁻²³ The individual wires were coupled to a common joint using a multichannel zero-resistance ammeter (ZRA) box and the current flowing through each individual electrode was independently measured. The common coupling joint was connected to the working electrode jack of a potentiostat so that the electrode array could be polarized to study the electrochemical spatiotemporal pattern of the electrode array at different potentials. With the 61-electrode array, it was shown (Figure 5) that (i) the activation (corrosion) of metal started at the center electrodes and propagated from the center to the edge and (ii) the passivation started from the edge electrodes and propagated in the opposite direction (from the edge to the center). By comparing the behavior of the total current from the electrode array with the behavior of the current from a one-piece electrode, the authors concluded that the array of electrodes behaved similarly to a one-piece electrode of the same shape and total area. Thus, the electrochemical spatial patterns observed with the electrode array are representative of patterns on a one-piece metal electrode. By using the coupled multielectrode array, the authors were able to determine directly the spatial pattern of the active-passive electrochemical oscillations and how the oscillation wave front travels on a large iron electrode. Hudson and coworkers conducted extensive studies in this area, and the results were reported in a large number of publications.²⁴⁻³⁹ Similar coupled multielectrode arrays were also used extensively by others to study the spatial interactions among the localized corrosion sites on stainless steel,⁴⁰⁻⁴⁵ and the localized corrosion behavior of aluminum alloys,⁴⁶⁻⁵² the characteristics of chromate coatings,⁵³ and atmospheric corrosion.⁵⁴ Coupled multielectrode systems were also used to study the deposition of metals.⁵⁵⁻⁵⁶

COUPLED MULTIELECTRODE ARRAYS FOR SPATIOTEMPORAL CORROSION MEASUREMENTS

Coupled multielectrode arrays (also called WBE) were used by Tan, et al., to study the spatiotemporal patterns of the localized corrosion current and potential on carbon steel electrodes.⁵⁷⁻⁶⁸ Their work with the coupled multielectrode arrays was first published in 1997.⁵⁷ Figures 6a and 6b show the multielectrode array used in their studies.⁵⁸ In Figures 6A and 6B, multiple electrodes were directly connected to a common joint. The current flowing through each electrode was measured by momentarily decoupling the electrode from the common joint and inserting a ZRA between the electrode and the common joint. The potential of the individual electrodes and the coupling joint was measured with a voltmeter (V) and a reference electrode (RE). Because the potential of each electrode was measured under open-circuit conditions, this system was not operating under truly coupled conditions. The decoupling of electrodes for the measurement of the open-circuit potential may have affected the ability for this system to simulate the behavior of a one-piece metal.

In a localized corrosion environment, each mini-electrode was considered to corrode uniformly and behave as an ideal electrochemical system because of the small size (3 to 4 orders of magnitude smaller than the electrode in a typical conventional corrosion probe such as a linear polarization probe). Therefore, the following formulae were derived on the basis of the Butler-Volmer equation to calculate the corrosion current on each electrode:⁵⁸

$$I_{ka} = I_{kcouple} / \{1 - \exp[-(2.3/b_{ka} + 2.3/b_{kc}) (E_{coup} - E_{kopen})]\} \quad (1)$$

where I_{ka} is the anodic current (or corrosion current) from electrode k ; $I_{kcouple}$ is the coupling current from electrode k measured with the ZRA; E_{kopen} is the open circuit potential of electrode k ; E_{coup} is the coupling potential of all the electrodes; and b_{ka} and b_{kc} are the anodic and the cathodic Tafel slopes, respectively. It was proposed to use a separate RE to measure the values for E_{kopen} , when electrode k is disconnected from the coupling joint, and E_{coup} . Linear polarization measurements were conducted to obtain the Tafel slopes.

It was hypothesized that if the value of $E_{coup} - E_{kopen}$ for an electrode is greater than 100 mV, the exponential term in Eq.1 will vanish, and the corrosion current from electrode k could be estimated by the coupling current from the electrode:

$$I_{ka} = I_{kcouple} \quad (2)$$

A system used to experimentally measure the coupling currents, coupling potential, open-circuit potential, and Tafel slopes is shown in Figures 6a, 6b, and 6c. Typical spatial distributions of the coupling currents and potential from the coupled multielectrode array are shown in Figure 7. It should be noted that the currents shown in Figure 7 were the coupling currents, $I_{kcouple}$, rather than the corrosion currents, I_{ka} , in Eqs. 1 and 2.

This method has been applied to mapping the localized corrosion behavior (coupled currents) of carbon steel materials in aqueous solutions⁵⁷, crevice,⁶⁴ water/gas interface,⁶⁵ and soil.⁶⁷ In localized corrosion conditions, electrode kinetics of actively pitting electrodes are often diffusion controlled and the kinetics of the passive electrodes are controlled by a thin oxide film. Because the Butler-Volmer equation applies to activation controlled processes, the application of Eq.1 to localized corrosion conditions should be evaluated. In addition, the decoupling of individual electrodes for the measurement of open-circuit potential or Tafel slope may alter the localized corrosion processes.

Tan and coworkers also used multielectrode arrays in conjunction with the electrochemical noise technique to measure the localized corrosion rate distributions.^{61,68} With this approach, the electrochemical noise resistances between paired electrodes in the multielectrode array were measured, and the localized corrosion rate for each electrode was calculated based on the electrochemical noise theory. Because the noise resistance was measured in pairs, the multielectrode array that operated under this mode was not a coupled multielectrode array.

COUPLED MULTIELECTRODE ARRAY SENSORS WITH ONE-PARAMETER OUTPUT FOR CORROSION MONITORING

The authors of this paper and their coworkers⁶⁹⁻⁹⁶ and other investigators⁹⁷⁻¹⁰² have used coupled multielectrode arrays as real-time sensors for monitoring the rate of corrosion, particularly localized corrosion. Figure 8 shows the principle of the CMAS.^{75,94,99} A resistor was used between each electrode and the common coupling point. Electrons from a corroding (or a relatively more corroding) electrode (or an anodic half-cell) flow through the resistor connected to the electrode and produce a small potential drop (usually in the microvolt levels for low currents). This potential drop is measured by the high-resolution voltage-measuring instrument and used to derive the currents. The CMAS probes can be made in several configurations and sizes, depending on the applications. Figure 9 shows some of the typical probes that were reported for real-time corrosion monitoring.

The data from these CMAS probes are the large number of current values measured at a given time interval from all the electrodes (see previous section). In a CMAS probe, these data are reduced to a single-parameter so that the probe can be conveniently used for real-time and online monitoring purposes, especially for industrial applications. The most anodic current has been used as a one-parameter signal for the CMAS probes.^{70,75} Because the anodic electrodes in a CMAS probe simulate the anodic sites on a metal surface, the most anodic current may be considered as the corrosion current from the most corroding site on the metal. The value based on three times of the standard deviation of currents is another way to represent the corrosion current from the most corroding site on the metal.⁷⁰⁻⁷⁵ Because the number of electrodes in a CMAS probe is always limited and usually far fewer than the number of corroding sites on the surface of a metal coupon, the value based on the statistical parameter, such as three times the standard deviation of current, was considered a better choice compared to the value of the most anodic current.^{70,75} The standard deviation value may be from the anodic currents or from both the anodic and the cathodic currents.⁷⁰⁻⁹¹

In a less corrosive environment or with a more corrosion-resistant alloy, the most anodic electrode may not be fully covered by anodic sites until the electrode is fully corroded. Therefore, the most anodic electrode may still have cathodic sites available, and the electrons from the anodic sites may flow internally to the cathodic sites within the same electrode. The total anodic corrosion current, I_{corr} , and the measured anodic current, I_a^{ex} may be related by^{70,75,89}

$$I_a^{\text{ex}} = \varepsilon I_{\text{corr}} \quad (3)$$

where ε is a current distribution factor that represents the fraction of electrons resulting from corrosion that flows through the external circuit. The value of ε may vary between 0 and 1, depending on parameters such as surface heterogeneities on the metal, the environment, the electrode size, and the number of sensing electrodes. If an electrode is severely corroded and significantly more anodic than the

other electrodes in the probe, the ε value for this corroding electrode would be close to 1, and the measured external current would be equal to the localized corrosion current.^{70,89}

Figure 10a shows typical responses of the standard deviation of the currents measured from a 25-electrode probe made of Type 304 stainless steel (UNS S30400).^{70,75} The following order of increasing corrosiveness was observed: deionized water < saturated KCl < 0.0025 M FeCl₃ < 0.25 M FeCl₃. Figure 10a also shows that NaNO₃ is an effective corrosion inhibitor for stainless steel in FeCl₃ solution.

The maximum localized corrosion penetration rate can be calculated using Faraday's law:^{70,75}

$$CR_{\max} = (1/\varepsilon)(I_{\text{corr}})W_e / (F\rho A) \quad (4)$$

$$W_e = 1 / \sum(m_i z_i / W_i) \quad (5)$$

where CR_{\max} is the estimated maximum penetration rate (cm/s), ε is the current distribution factor; σ is the standard deviation of currents (A); F is the Faraday constant (96485 C/mol); A is the surface area of the electrode (cm²); ρ is the density of the alloy or electrode (g/cm³); W_e is the equivalent weight (g/mol) as defined by Eq. 5; and m_i , z_i , and W_i are the mass fraction of each alloying element in the alloy, oxidation state of the alloying element in solution, and atomic weight of alloying element, i , in the alloy, respectively. Eq. 4 assumes that corrosion on the most corroded electrode is uniform over the entire surface. Because the electrode surface area is usually between 0.01 and 0.0003 cm², which is approximately 2 to 4 orders of magnitude less than that of a typical LPR probe or a typical electrochemical noise (EN) probe, the prediction of penetration rate or localized corrosion rate by assuming uniform corrosion on the small electrode is realistic in most applications.^{70,75}

Figure 10b shows typical responses of the maximum localized corrosion rate (derived from the most anodic current) of a low carbon steel CMAS probe measured by a commercial instrument.⁹⁸ The maximum localized corrosion rate in air was close to the instrument theoretical detection limit (10 nm/yr). The initial maximum localized corrosion rate was 10 μ m/yr in distilled water. The maximum localized corrosion rate in simulated seawater was approximately 1 mm/yr. When 10 mM H₂O₂ was added to the simulated seawater, the corrosion rate was 10 mm/yr. It was later verified that the corrosion of the electrode in the distilled water and in the simulated seawater were mainly in the form of pitting corrosion.⁹⁴ Therefore, the maximum corrosion rate in Figure 10b represents the maximum pitting rate.

APPLICATIONS OF CMAS FOR REAL-TIME CORROSION MONITORING

CMAS probes have been extensively used for monitoring localized corrosion of a variety of metals in the following environments:

- Cooling water^{71,75,86,91}
- Simulated seawater⁹³
- Salt-saturated aqueous solutions⁷⁶
- Concentrated chloride solutions⁷²
- Concrete⁹⁹
- Soil¹⁰⁰
- Low-conductivity drinking water⁹⁴
- Process streams of chemical plants at elevated temperatures^{79,83,88}

- Coatings^{97,101}
- Deposits of sulfate-reducing bacteria^{78,85}
- Deposits of salt in air^{77,81}
- High pressure simulated natural gas systems⁹⁶
- H₂S systems⁹⁶
- Oil/water mixtures⁹⁰

The CMAS probes were also used in cathodically protected systems for the effectiveness of cathodic protection.⁹⁸ In addition, CMAS probes have been used to measure the propagation rate of metals in crevice.⁹² Some of these applications are summarized in the following sections.

Corrosion of Alloys in Chloride Solutions

CMAS probes were used for comparing localized corrosion of Fe-Ni-Cr-Mo alloys in chloride solutions.⁷² Experimental results indicated that CMAS probes provided a rapid real-time response to changes in temperature and salt concentration. The nonuniform corrosion resistance of the alloys in all tested solutions was found to increase in the following order: carbon steel < Alloy 600 (UNS N0600) < Type 304 SS (UNS S30400) < Type 316 SS (UNS S31600) < Alloy 276 (UNS N10276) < Alloy 22 (UNS N06022). This order is consistent with the pitting resistance equivalent numbers calculated according to the elemental composition of the alloys and the experiences with these alloys in the industries. Similar measurements were also conducted for Types 1100 and 3003 aluminum (UNS A91100 and A93003); Types 304L (UNS S30403), 316L (UNS S31603), 904L (UNS N08904), and 254 SMO (UNS S31254) stainless steel; and Type 110 copper (UNS C11000) in simulated seawater.⁹³

Corrosion in Sulfate-Reducing Bacteria Solutions

Microbially influenced corrosion of carbon steel and stainless steel by sulfate-reducing bacteria was measured with CMAS probes in simulated seawater.^{78,85} Figure 11 shows a comparison of the maximum localized corrosion currents from a probe in the cells with and without sulfate-reducing bacteria (SRB) and a comparison of the post test appearances of the sensing electrodes of the probes in the two cells.⁷⁸ Approximately one week after the introduction of the SRB, the corrosion current from the cell where SRB was present was approximately one order of magnitude higher than that from the cell where SRB was absent. The post test pictures clearly show that the sensing electrodes of the probe in the SRB cell were more corroded than those of the probe in the control cell. Pitting corrosion in the SRB cell was also evident.

Corrosion under Biofilms

Corrosion under biofilms in a high-pressure natural gas system was evaluated with two CMAS probes.⁹⁶ Figure 12 shows the two probes (one covered with sulfate-reducing bacteria deposits and the other covered by corrosion products formed in an H₂S-containing water) and the localized corrosion rates measured from each probe when the relative humidity changed. Initially, the relative humidity was maintained below 30% for more than 10 days. The localized corrosion rate from the precorroded probe was low (<0.001 mm/yr), while the localized corrosion rate from the SRB deposits covered probe was never below 0.1 mm/yr. Increasing the relative humidity caused the localized corrosion rate from the precorroded probe to increase rapidly after the relative humidity passed approximately 38%. The localized corrosion rate of the SRB deposits covered probe also increased when the relative humidity reached approximately 45%. At relative humidities above 70%, the localized corrosion rate from the SRB deposits covered probe remained higher than that from the precorroded probe. This measurement

demonstrated that once contaminated by SRB deposits, it is difficult to stop the corrosion even at relative humidities lower than 30% because of the hygroscopic nature of the SRB deposits or the electrolyte trapped beneath the deposits. It should be mentioned that the relative humidity values at which the corrosion rates started to increase might have been different if the relative humidity had changed slower.

Corrosion Under Salt Deposits in Air

The nonuniform corrosion rates of carbon steel and stainless steel were measured with CMAS probes under salt deposits in air^{77, 81} and in saturated aqueous solutions.⁷⁶ Figure 13 shows the experimental setup and typical results obtained with a carbon steel CMAS probe under initially pure KCl salt powder in air as a function of relative humidity.⁷⁷ Figure 13 indicates that the critical relative humidity (CRH) for corrosion to initiate was 67%, which was lower than the deliquescence relative humidity (DRH) of the KCl salt (81%). Figure 13 also shows that, once initiated, the corrosion did not stop when the relative humidity was decreased to 27%, a value that is much lower than the initial CRH. This phenomenon was attributed to the formation of corrosion products that lowered the original DRH and the CRH.

Corrosion in Pressurized Streams of a Chemical Plant at Elevated Temperatures

CMAS probes were used to measure the localized corrosion rates of process piping materials in a chemical plant.^{79, 83} Figure 14 shows the probes in a side circuit of a pressurized process stream at elevated temperatures and typical real-time results from the *in-situ* monitoring of the corrosion currents during the initial 4-day test. As expected, the corrosion current density of the Type 316L stainless steel was much higher (corresponding to 8 mm/yr) than those from AL6X+N (UNS N08367) and Alloy 276. Subsequent visual examination of the probes confirmed the localized corrosion of the Type 316L stainless steel. The post test-measured corrosion rates were in reasonable agreement with the rate predicted from the current measurements. The measured results are also consistent with the model predictions for localized corrosion.⁸⁸

Corrosion in the Cooling Water System of Chemical Plant

CMAS probes were used to measure the localized corrosion rates of cooling water piping materials in a chemical plant.⁸⁶ Figure 15 shows (i) the monitoring station for cooling water corrosivity and chemistry where CMAS probe were installed and (ii) typical real-time results from two carbon steel CMAS probes during a 5-month test. A high localized corrosion rate was observed. Figure 16 shows the post test appearance of the sensing electrodes of a probe and two carbon steel coupons tested in the same monitoring station. The maximum pitting rate [3.73 mm/yr (149 mil/yr)] according to the corroded depth mentioned in Figure 16 is consistent with the real-time average maximum localized corrosion rate from the probe [(3.62 mm/yr (145 mil/yr); see Figure 15). The measured localized corrosion rate was also consistent with the pitting rate measured from the coupons tested in the same water [2.5 to 5 mm/yr (100 to 200 mil/yr); see Figure 16].

Corrosion in Crude Oil and Water Mixtures

CMAS probe was used to measure the localized corrosion of carbon steel in crude oil containing small amounts of brines.⁹⁰ Figure 17 shows the typical real-time results from a carbon steel CMAS probe at room temperature. The localized corrosion rate signal (current) was low (<1 nA) when the probe was in dry air and in the desalted crude oil. After a small amount of 0.5 M NaCl solution was

added, the corrosion signal increased from 1 nA to approximately 1 μ A. This measurement demonstrated that even if the sensing electrodes of the probe were coated with a layer of crude oil, the probe responded to the corrosivity of the crude oil when the corrosive brine was added, and the response was instantaneous.

Evaluation of Corrosion Inhibitors

CMAS probes were used to evaluate the performance of several types of corrosion inhibitors for carbon steel in a simulated cooling water environment in a laboratory.⁷¹ Figure 18 shows a typical response of the CMAS probe to the dosing of a commercial inhibitor. The probe provided a quantitative measurement of localized corrosion currents and a rapid real-time response to the dosing of the inhibitor. The response of the probe to both inhibitor type and inhibitor concentration provided useful information in the selection of the types and the dosing of the inhibitors.⁷¹

Evaluation of Coatings and Monitoring Degradation of Coatings

CMAS probes were used to evaluate the quality and to monitor the degradation of coatings. CMAS probes made of carbon steel were painted with different types of commercial coatings (Figure 19).^{97,101} The electrode tips of selected probes were mechanically scratched to simulate the initial defects (pinholes) on the coating. All probes were immersed in simulated seawater and tested at 26 °C. A multichannel CMAS analyzer was used to simultaneously measure the signals from the different probes. Figure 19 presents the corrosion signal changes measured from the coated probes in response to the initial defects and the degradation of the coatings. Signals from the probes with simulated initial defects on coatings (Probe #1 had three coating-damaged electrodes and Probe #2 had eight coating-damaged electrodes) increased instantaneously from the lower detection limit (2×10^{-11} A) to more than 1×10^{-6} A upon immersion in the brine and remained above 1×10^{-6} A throughout the test. The signals from the probes with poor quality coatings (Probes #4 and #6) increased either instantaneously upon immersion in the brine or gradually after immersions in the brine. The signal from the probe with high quality coating (Probe #5) remained at the background noise value (2.2×10^{-11} A; Figure 19) throughout the experiment. The sudden increase in the probe #4 signal shows the response to a rapid degradation (cracking and peeling of the coating).⁹⁷

Corrosion Under Cathodic Protection Conditions

CMAS probes were used to monitor the effectiveness of cathodic protection (CP) for carbon steels.⁹⁸ Figure 20 shows how the probes were connected to the cathodically protected systems and the measured results from two CMAS probes. The localized corrosion rates were exceptionally high (>10 mm/yr) when the potential increased, which simulated the condition when the CP polarity was incorrectly connected. The localized corrosion rate decreased with the decrease of the potential and became essentially zero when the CP potential reached the critical CP potential [-0.72 to -0.74 V(SCE)]. The corrosion rates shown in Figure 20 represented the corrosion rate of the most anodic electrode. Compared with a large single electrode probe which gives average corrosion rate over a large surface area, the multielectrode probe indicates the CP conditions in which the worst section of a metal is statistically protected.

Corrosion in Concrete and Soil

CMAS probes were used to monitor the localized corrosion of carbon steel in concrete⁹⁹ and in soil.¹⁰⁰ Figure 21 shows the experimental setup used for the measurement in concrete.⁹⁹ Two carbon

steel probes and aluminum wires were embedded in the concrete. The aluminum wires were used as sacrificial anodes for cathodic protection during the later stage of the experiment (not shown here). Figure 22 shows the localized corrosion rates from one of the probes. Initially, the corrosion rate was high, but decreased to about 2 $\mu\text{m}/\text{yr}$ in 2 days. After the setting of the concrete that was prepared with distilled water, the concrete was partially immersed in simulated seawater. The localized corrosion rate increased slightly two days after the immersion in simulated seawater, probably due to the arrival of chloride by diffusion. Shortly after the slight increase, the localized corrosion rate decreased gradually over the 1-month experiment.

Figure 23 shows the localized corrosion rates measured from a carbon steel CMAS probe in soil (in a similar setup as shown in Figure 21).¹⁰⁰ During the test, the soil was partially immersed in distilled water or simulated seawater. Unless otherwise noted, the probe was surrounded by densely packed soil (mud). The localized corrosion rate increased significantly when the probe was raised from the soil, and a liquid-filled space was formed at the sensing tip of the probe. The corrosion rate was low when the probe was placed at a location above the liquid level, and the soil was loose. The localized corrosion rate increased instantly, but decreased rapidly after it was pressed into the densely packed clay soaked either by distilled water or by simulated seawater. The low corrosion rate in the densely packed soil was attributed to mass transfer limitations in the densely packed clay.

Corrosion in High-Pressure Gas Systems

The CMAS probes were used to monitor the corrosion of carbon steel materials in a simulated natural gas system at a pressure of 34 atm (500 psi).⁹⁶ Figure 24 shows the experimental setup and test results. The composition of the simulated natural gas was $\text{N}_2(\text{balance})+1\%\text{CO}_2+0.1\%\text{O}_2+0.01\%\text{H}_2\text{S}$. The measured localized corrosion rate from the carbon steel CMAS probe was approximately 0.08 mm/yr in the N_2 gas when the relative humidity was 95% and 0.11 mm/yr in the simulated natural gas when the relative humidity was only 75%. The localized corrosion rate dropped below 0.001 mm/yr when the relative humidity was below 25% in both the N_2 and the natural gases. Therefore, relative humidity is the most important factor in controlling the corrosion in natural gas systems.

Corrosion in H_2S Systems and the Bridging Effect by Electronic-Conducting Corrosion Products

CMAS probes were used to monitor the corrosion of carbon steel materials in solutions saturated with 100% H_2S at ambient temperature and pressure.⁹⁶ Figure 25 shows the results measured with two sets of CMAS analyzer units. The first analyzer used larger resistors as the coupling resistors, and the second analyzer used smaller resistors as the coupling resistors (see Figure 8). The localized corrosion rate was high initially, but decreased gradually with time when the probe was connected to the instrument unit that had large resistors. Because the corrosivity of the solution should not decrease after introducing the H_2S , the decrease in the measured corrosion rate was apparently caused by the bridging effect (i.e., some localized corrosion electrons flowing through the electronic-conductive corrosion products, such as FeS , built-up on the sensing surface). At the end of the experiment, the DC resistance measurement between each electrode and the coupling joint showed a significant decrease (from several megaohms to less than 100 ohms) which indicates the bridging effect. However, when the localized corrosion rate for the same probe was measured with the second analyzer that had lower values of coupling resistors, the localized corrosion rate was close to the value measured initially when no corrosion products were built-up. Therefore, the CMAS probe works in H_2S environments as long as the coupling resistors are low.

This bridging phenomenon affects most probes that are based on electrochemical principle, such as the LPR probe, and the ER or inductance principle, such as the ER probe. Unlike the LPR and the ER probes, which apply an external voltage and measure the responding current that may partially flow through the bridging circuit, the CMAS method does not apply the external voltage; it measures the current that is produced by the intrinsic, naturally occurring corrosion reactions at the corroding sites. If the resistance value in the instruments is significantly lower than that of the bridging circuit, most of the currents produced by the naturally occurring corrosion reactions would flow through the instrument, rather than through the bridging circuit, and they would be detected.

Corrosion in Extremely Low-Conductivity Water

The measurements of corrosion in low-conductivity water have been a challenge to some of the electrochemical methods, such as the LPR probe, even though more advanced instruments have been designed to compensate for the solution resistance effect. Figure 26 shows the localized corrosion rate in distilled water measured with CMAS probes.⁹⁴ The conductivity of the distilled water is extremely low initially, but may increase slightly during the measurement because of the absorption of CO₂ from the open air. CMAS probe functions well in the low-conductivity water because it does not need externally applied voltage perturbation; it measures the current under naturally occurring conditions. It may be necessary, though, that the electrodes in the CMAS probe should be closely packed for more accurate results. No literature report is available to show the electrode spacing effect in low-conductivity water.

Corrosion Under Crevice

CMAS probes have been used to measure the localized corrosion rate under crevice. Figure 27 shows the typical creviced CMAS probes and a comparison of the measured maximum localized corrosion rates from a creviced probe and from a regular uncreviced probe in simulated seawater for Type 1008 carbon steel.⁹² The crevice was formed by imbedding a layer of paper between the sensing surface and epoxy, and the tightness of crevice was controlled by selecting the thickness of the paper. The corrosion rate from the creviced probe was found to be an order of magnitude lower than that from the uncreviced probe. The low localized corrosion rate from the creviced probe was attributed to the mass transfer of the corrosion reactants and products within the crevice. Under the usual crevice corrosion condition, crevice corrosion involves the electron transfer from the crevice to the cathodic area outside of the crevice on the metal. To simulate this condition, the authors placed a large bare metal that was identical in composition to the electrodes of the CMAS probe near the creviced probe and electrically coupled the large bare metal to the common joint of the creviced CMAS probe. Interestingly, the localized corrosion rate from the creviced probe was essentially zero; the electrodes in the crevice were cathodically protected by the large bare metal which was more active and had lower open-circuit potential than the electrodes in the crevice.⁹²

IMPROVEMENTS ON CMAS INSTRUMENTATIONS FOR REAL-TIME CORROSION MONITORING

CMAS probes may be affected by the internal cathodic sites on the most corroding electrode that would cause the electrons resulted from corrosion to flow internally, which cannot be measured by the external circuit. In addition, the corrosion rates reported by the CMAS instruments mostly have been the localized corrosion rates that are not usually available in literature and cannot be conveniently compared with the general corrosion results obtained by other researchers. The following sections discuss the recent developments that were aimed to improve these limitations.

Internal Current Effects

Figure 28 shows the electron flow paths on the different kinds of electrodes in a CMAS probe.⁸⁹ If the most anodic electrode on a probe in a given environment is a partially corroded electrode (Figure 28b) rather than a totally corroded active electrode (Figure 28a), it would still have the cathodic sites to accept electrons from the neighboring anodic sites on the same anode.^{70,75} The total anodic current or total corrosion current, I_{corr} (see Eq. 3), is the sum of the external anodic current, I_a^{ex} , and the internal anodic current, I_a^{in} , that flows from the cathodic sites within the electrode:

$$I_a = I_a^{\text{ex}} + I_a^{\text{in}} \quad (6)$$

The CMAS probe relies on the measurement of the external anodic current to estimate the nonuniform corrosion rate according to Eq. 3. In Figure 28a, the electrode is totally active and fully corroded; all or most of its corrosion electrons flow to the other electrodes through the external circuit, and the corresponding ε (Eq. 3) is equal or close to unity. On the other hand, in Figure 28b, the electrode is partially corroded; a portion of its corrosion electrons flow to the local cathodic sites, and the corresponding ε is less than 1. Therefore, in the case of Figure 28b, there is uncertainty with using the CMAS probe to predict the corrosion rate if ε is assumed to be unity.

The coupling potential, E_{coup} , and the polarization behavior of an individual electrode determine whether an electrode in a CMAS probe or a reaction site on an electrode is anodic or cathodic. If the most anodic electrode is fully corroded (or totally active) (Figure 28a), the potential of all the sites on the electrode would be lower than E_{coup} , therefore, there is no internal current ($I_a^{\text{in}} = 0$). If, however, the most anodic electrode is only partially corroded (Figure 28b), some reaction sites on this electrode may have a potential that is higher than E_{coup} , and the internal current, I_a^{in} , will be nonzero.

Because the multiple electrodes in a CMAS probe simulate the different cathodic and anodic sites of a metal coupon, the highest potential (usually the potential measured from the most cathodic electrode) can be considered to statistically represent the potential of the most cathodic site on the metal (after it is electrically isolated from the other sections of the metal). The potential measured from the most cathodic electrode may thus be considered as the highest bounding potential for all the cathodic sites on the most anodic electrode. Therefore, if the coupling potential of a CMAS probe is raised to a value that is slightly higher than the potential measured from the most cathodic electrode, there should be no cathodic reaction on the most anodic electrodes even though some areas are still uncorroded. Under these conditions, $\varepsilon \rightarrow 1$ and $I_a^{\text{in}} \rightarrow 0$ (Eqs. 3 and 6), the uncertainty in the measured corrosion rate from the CMAS probe due to I_a^{in} can be eliminated.

A polarization unit, as shown in Figure 29, was proposed for a CMAS instrument to dynamically adjust the potential of the coupling joint of the probe such that the currents from the most cathodic electrode of the CMAS probe is slightly anodic (lower than zero if an anodic current is recorded as a negative current by the instrument or higher than zero if a cathodic current is recorded as a negative current by the instrument). Under this condition, the coupling potential is higher than the open-circuit potential of the most cathodic electrode.

Because raising the coupling potential also increases the current from the active sites, the corrosion rate measured at the raised coupling potential may be higher than the actual corrosion rate. Thus, the corrosion rate measured at the raised coupling potential may be considered the upper bound of corrosion rate. The corrosion rate measured at the natural coupling potential, E_{coup} , may be considered

the lower bound of corrosion rate because of the possible nonzero internal flow of electrons on the most corroding electrode at E_{coup} . This upper bound is a realistic value because the raised coupling potential is an actual value measured from one of the electrodes of the probe.

Preliminary measurements were conducted in a 0.5 M NaCl solution using the improved CMAS method as shown in Figure 29.⁸⁹ The upper bounds of the maximum localized corrosion rates were found to be 2.2 to 2.7 times higher than the lower bounds for the probes made of Alloy 276, Type 316 stainless steel, and Type 1008 carbon steel, respectively. Therefore, the maximum localized corrosion rate values measured at the natural coupling potential were close to the actual maximum localized corrosion rates for these three metals in 0.5 M NaCl solution.

General Corrosion

The maximum localized penetration rate and cumulative maximum localized penetration depth are important parameters for the assessment of localized corrosion. However, the maximum penetration rates for alloys are rarely available, and the measured localized corrosion rates by the CMAS probes cannot be easily compared with the general corrosion rates commonly reported in literature. In addition, maximum penetration rate is difficult to measure, whereas general corrosion rate can be measured by many methods, such as the LPR and ER probes, or weight loss methods.

In most cases, localized corrosion is associated with some degree of general corrosion. When a metal is undergoing corrosion, the corroding metal is usually at an electrochemical potential (corrosion potential) that is significantly higher than the metal's deposition potential. Thus, the cathodic currents do not directly contribute to the metal loss or the metal gain, and therefore can be ignored in the corrosion rate calculation. For this reason, the average corrosion penetration rate may be calculated using the average value of the anodic currents from the CMAS probe.⁹³

$$I_{\text{avg}}^{\text{a}} = (\sum I_i^{\text{a}})/n, \text{ i from 1 to n} \quad (7)$$

where I_i^{a} is the anodic current from the i^{th} electrode, n is the number of electrodes in the probe, and $I_{\text{avg}}^{\text{a}}$ is the average of the anodic currents. If I_i^{a} is cathodic, it is set to zero in the summation. Thus, the average corrosion rate, CR_{avg} , may be calculated by⁹³

$$\text{CR}_{\text{avg}} = (1/\varepsilon)I_{\text{avg}}^{\text{a}}W_e/(F\rho A) \quad (8)$$

The general corrosion penetration rate obtained using the weight loss method or by an electrochemical method using relatively large electrodes is essentially the corrosion rate averaged over the sample surface area. Therefore, Eq. 8 can be used to estimate the general corrosion rate if there is no internal current effect.

The localized corrosion rate factor, f_{rate} , was defined as the ratio of the maximum localized corrosion rate to the average corrosion penetration rate. It can be expressed by⁹³

$$f_{\text{rate}} = \text{CR}_{\text{max}}/\text{CR}_{\text{avg}} \quad (9)$$

The localized corrosion rate factor indicates how much higher the localized corrosion rate (e.g., the penetration rate of the fastest growing pit on the surface of a coupon in the case of pitting corrosion) is than the average corrosion rate (e.g., the average penetration rate on the surface of a coupon). It should be noted that the maximum localized corrosion rate may not always be found on one electrode. In

a CMAS probe, one electrode may have the highest corrosion rate at one time, but another electrode may corrode at the highest rate at another time.

Similar to the average corrosion rate, the average anodic charge, Q_{avg}^a , may be calculated by⁹³

$$Q_{avg}^a = (\sum Q_i^a)/n, \text{ i from 1 to n} \quad (10)$$

where Q_i^a is the anodic charge from the i^{th} electrode, and n is the number of electrodes in the coupled multielectrode probe. If the value of Q_i^a is cathodic, it is set to zero in the summation. Thus, the average corrosion penetration depth, H_{avg} , may be calculated by⁹³

$$H_{avg} = (1/\varepsilon)(Q_{avg}^a)W_e/(F\rho A) \quad (11)$$

Similar to the average corrosion rate, Eq. 11 can be used to estimate the general corrosion penetration depth.

The localized penetration depth factor, f_{depth} , may be defined as the ratio of the maximum localized penetration depth to the average corrosion penetration depth⁹³

$$f_{depth} = H_{max}/H_{avg} \quad (12)$$

The localized corrosion penetration depth factor indicates severity of localized corrosion depth (e.g., the deepest penetration of the most corroded pit on the surface of a coupon in the case of pitting corrosion) compared to the general corrosion penetration or the average corrosion penetration (e.g., the average loss in thickness on the surface of a coupon). Similar to the localized corrosion rate, the maximum penetration may not always be found on the same electrode. It also might not be found on the electrode that has the highest penetration rate at a given time. Instead, the electrode that has the highest cumulative penetration has the maximum penetration depth.

Figure 30 shows the typical measured maximum localized corrosion rate, the average corrosion rate (which was used to estimate the general corrosion rate), the maximum localized penetration depth, and the average penetration depth (which was used to estimate general corrosion depth) measured using a Type 3003 aluminum CMAS probe in simulated seawater.⁹³ The corrosion rate was near the background noise level (0.1 $\mu\text{m}/\text{yr}$) in the air. As soon as the probe was placed in the simulated seawater, the maximum pitting penetration rate changed to 0.52 mm/yr and fluctuated between 0.154 and 1.68 mm/yr. The average corrosion rate was between 0.035 and 0.16 mm/yr. The maximum pitting rate in simulated seawater averaged over the testing period was 584 $\mu\text{m}/\text{yr}$, and the average corrosion rate in the simulated seawater (or estimated general corrosion rate) averaged over the testing period was 75 $\mu\text{m}/\text{yr}$. The overall localized corrosion rate factor (ratio of the maximum pitting rate to the average corrosion rate, both averaged over the testing period) was 7.83. The final localized corrosion depth factor was 5.02.

LIMITATIONS OF MULTIELECTRODE SYSTEMS

All electrochemical techniques have limitations. Coupled electrode systems, depending on their operating principles, have their own limitations. Corrosion engineers need to understand these limitations in order to use them effectively for research or monitoring. As previously discussed, an obvious limitation of the CMAS probe is the underestimation of actual dissolution rates because of concurrent cathodic reactions occurring on the most anodic electrode of the array. The corrosion rate

from an unpolarized CMAS probe may be lower than the actual corrosion rate and is the lower bound of the corrosion rate. The proposed method to overcome this limitation is to slightly polarize the probe to or near the potential of the most cathodic electrode. This polarization method gives the upper bound of the corrosion rate. Although the tests with selected systems showed that the lower bound values were close to the upper bound values (factor of 2.2 to 2.7), the lower and upper bound values may be significantly different for other systems. An alternative approach is to use small electrodes, because the smaller the electrode, the greater the chance of anodic reactions completely covering an electrode surface. This, however, may not be practical for all situations. In addition, if the electrode is too small, it may no longer represent the corrosion behavior of a large metal. The electrode size effect should be determined before any attempt to use extremely small electrodes.

A second limitation of the CMAS probe is that although it provides quantitative rate information, it does not provide a “signature” for a given corrosion process. The dispersion in an individual electrode current may be used as a measure of localization of corrosion, but this is the degree of localization rather than a “signature”. The use of WBE in the noise mode may enable the probe to provide a signature for different corrosion modes, but this method needs to be further explored.

A third limitation, especially for purposes of research in localized corrosion phenomena, is the crevice between each electrode and the surrounding insulator. Although different methods and different types of epoxy or paints have been used to reduce or eliminate the formation of crevices, the fabrication of a crevice-free multielectrode probe for certain environments, especially under elevated temperature conditions, has been a challenge. For a less corrosion-resistant metal in a corrosive environment, such as carbon steel in seawater, this may not be an issue because corrosion takes place mostly on the boldly exposed metal surfaces. For corrosion-resistant metals, however, the formation of crevices makes interpretation of crevice corrosion between the electrode array and a controlled crevice difficult because the origin of the current is not localized to one crevice. Furthermore, the area of corrosion is less defined, and the calculation of corrosion rates may be difficult if crevice forms.

Finally, because the electrode areas are small and low levels of current are measured, precautions must be taken to minimize noise from thermal junctions, dissimilar electrode contacts, and other noise sources. Care must also be taken in the electrode preparation to ensure that the metallurgical state of the actual material of interest is adequately represented by the electrodes. Often, wires of an alloy do not have the same microstructure as other wrought forms.

SUMMARY

Coupled multielectrode systems have been used for qualitative corrosion detection in concrete for nearly two decades and for crevice corrosion detection for more than 13 years. Coupled multielectrode arrays with spatially patterned electrodes have been used for electrochemical studies for at least 10 years. The coupled multielectrode arrays that can be arranged in any given patterns have been used by many researchers for studying the spatial patterns and the electrochemical behaviors of the corrosion processes, especially the localized corrosion processes of metals.

With the advancement of the coupled multielectrode arrays and multichannel instrumentation, real-time CMAS probes have been developed. These probes give simple parameters, such as maximum localized corrosion rate, maximum localized corrosion penetration depth, and average corrosion rate. The CMAS probes have been extensively used for online and real-time corrosion monitoring in laboratories and industrial fields. Because CMAS probes do not require the presence of bulk electrolytes, they have been used not only in aqueous solutions, but also in wet gases, oil/water mixtures,

salt deposits, biodeposits, soil, concrete, and undercoatings. CMAS probes also have been used for real-time monitoring of the effectiveness of cathodic protection in cathodically protected systems. In addition to the real-time measurement of the quantitative rate of localized corrosion, such as pitting and crevice corrosion, CMAS probes have also been used to estimate the general corrosion rate based on the average corrosion rate. With proper design in seals and access fittings, CMAS probes also have been used for corrosion monitoring at high-pressure and elevated temperatures.

ACKNOWLEDGMENTS

The authors acknowledge the reviews of Dr. P. Shukla, Dr. B. Sagar, and E. Hanson, and the assistance of C. Patton in preparing the manuscript.

REFERENCES

1. P. Schiessl, United States Patent 5,015,355, "Corrosion Measuring Cell," May 14, 1991.
2. P. Schiessl, Federal Republic of Germany Patent Application 3,834,628, "Corrosion Measuring Cell," October 11, 1988.
3. P. Schiessl and M. Raupach, "Monitoring System for the Corrosion Risk for Steel in Concrete," *Concrete International*, No. 7 (1992): p. 52-55.
4. P. Schiessl and M. Raupach, "New Approach for Monitoring of the Concrete Risk for the Reinforcement- Installation of Sensors," *Proceedings, International Concrete: Across Borders*, Odense, Demark, June, 1994, p. 65-78.
5. R. Bassler, J. Mietz, M. Raupach, O. Klinghoffer, "Corrosion Risk and Humidity Sensors for Durability Assessment of Reinforced Concrete Structures," *Proc. EUROCORR 2000*, London, article 100805 (2000).
6. R. Bassler, J. Mietz, M. Raupach, O. Klinghoffer, "Corrosion Monitoring Sensors for Durability Assessment of Concrete Structures," *Proc. SPIEs 7th Internat. Symp. on Smart Structures and Materials*, Newport Beach, article 3988 06 (2000).
7. R. Bassler, J. Mietz, M. Raupach, O. Klinghoffer, "Corrosion Monitoring Sensors for Durability Assessment of Concrete Structures," *Proc. SPIEs 7th Internat. Symp. on Smart Structures and Materials*, Newport Beach, article 3988 06 (2000).
8. O. Klinghoffer, P. Goltermann, and R. Bassler, "Embeddable Sensors for Use in the Integrated Monitoring Systems of Concrete Structures," *First International Conference on Bridge Maintenance, Safety and Management IABMAS 2002*, Barcelona, July 14-17, (2002).
9. U. Steinsmo, "The Effect of Temperature on Propagation of Crevice Corrosion of High Alloyed Stainless Steel in Natural Seawater," *Progress in the Understanding and Prevention of Corrosion*, 10th Eur. Corros. Congr. Paper, Volume 2, J. M. Costa, and A. D. Mercer, Ed, Institute of Materials, London, UK, 1993, p. 974-982.

10. U. Steinsmo, T. Rone, and J. M. Drugli, "Aspects of Testing and Selecting Stainless Steels for Sea Water Applications," CORROSION/94, paper no. 492, (Houston, TX: NACE International, 1994).
11. U. Steinsmo, T. Rogne, and J. Drugli, "Aspect of Testing and Selecting Stainless Steels for Seawater Applications," Corrosion, 53, 12, (1997): p 955-964.
12. U. Steinsmo, "Test Method for Localized Corrosion of Stainless Steel in Sea Water," Pitture Vernici Europe, 74, 14, (1998): p. 15-18.
13. Y.J. Tan, "The Effect of Inhomogeneity in Organic Coatings on Electrochemical Measurements Using a Wire Beam Electrode, Part 1," Progress in Organic Coatings, 19, (1991): p. 89- 94.
14. Y..J. Tan and S.T. Yu, "The Effect o Inhomogeneity i Organic Coatings on lectrochemical Measurements Using a Wire Beam Electrode, Part 2," Progress in Organic Coatings, 19, (1991): p. 257-263.
15. Y.J. Tan, "A New Crevice Corrosion Testing Method and Its Use in the Investigation of Oil Stain," Corrosion, 50, 4, (1994): p. 266-269.
16. Q. Zhong, "Electrochemical Technique for Investigating Temporarily Protective Oil Coatings," Progress in Organic Coatings, 30, 4, (1997): p. 213-218.
17. Q. Zhong, "Wire Beam Electrode: A New Tool for Investigating Electrochemical Inheterogeneity of Oil Coating," Progress in Organic Coatings, 30, 4, (1997): p. 279-285.
18. Z. Qingdong, "A Novel Electrochemical Testing Method and Its Use in the Investigation of Underfilm Corrosion of Temporary Protective Oil Coating," Corrosion, 56, 7, (2000): p. 722-726.
19. Q. Zhong, "Potential Variation of a Temporarily Protective Oil Coating before Its Degradation," Corrosion Science, 43, 2, (2001): p. 317-324.
20. Q. Zhong, "Study of Corrosion Behaviour of Mild Steel and Copper in Thin Film Salt Solution Using the Wire Beam Electrode," Corrosion Science , 44, 5, (2002): p. 909-916.
21. Q. Zhong, "A Novel Electrochemical Testing Method and Its Use in the Investigation of the Self-Repairing Ability of Temporarily Protective Oil Coating," Corrosion Science, 44, 6, (2002): p. 1247-1256.
22. Q. Zhong, Z. Zhao, "Study of Anti-Contamination Performance o Temporarily Protective Oil Coatings Using Wire Beam Electrode," Corrosion Science, 44, 12, (2002): p. 2777-2787.
23. Z. Fei, R. G. Kelly, and J. L. Hudson, "Spatiotemporal Patterns on Electrode Arrays," J. Phys. Chem., 100, (1996): p. 18986-18991.
24. Z. Fei, "Spatiotemporal Behavior of Iron and Sulfuric Acid Electrochemical Reaction System," PhD Thesis, University of Virginia, Charlottesville, Virginia, Diss. Abstr. Int., B 1997, 58, 3, 1402, May, 1997.

25. Z. Fei and J.L. Hudson, "Pacemaker-Driven Spatiotemporal Patterns on an Electrode Array," *Journal of Physical Chemistry B*, 101, 49, (1997): p. 10356-10364.
26. Z. Fei and J. L. Hudson, "Chaotic Oscillations on Arrays of Iron Electrodes," *Industrial & Engineering Chemistry Research*, 37, 6, (1998): p. 2172-2179.
27. J.L. Hudson, "Spatiotemporal Patterns in Electrochemical Systems," in *Pattern Formation in Continuous and Coupled Systems*, IMA Volume in Mathematics and its Applications 115, p.137-146, Martin Golubitsky, Dan Luss, and Steven H. Strogatz, eds., Springer, (1999).
28. Z. Fei, B.J. Green, and J.L. Hudson, "Spatiotemporal Patterns on a Ring Array of Electrodes," *Journal of Physical Chemistry B*, 103, 12, (1999): p. 2178-2187.
29. I. Z. Kiss, W. Wang, and J. L. Hudson, "Experiments on Arrays of Globally Coupled Periodic Electrochemical Oscillators," *J. Phys. Chem. B*, 103, (1999): p. 11433-11444.
30. W. Wang, I. Z. Kiss, J.L. Hudson, "Experiments on arrays of Globally Coupled Chaotic Electrochemical Oscillators: Synchronization and Clustering," *Chaos*, 10, 1, (2000): p. 248-256.
31. I.Z. Kiss, G. Vilmos, and J. L. Hudson, "Experiments on Synchronization and Control of Chaos on Coupled Electrochemical Oscillators," *J. Phys. Chem. B* 104, (2000): p. 7554-7560.
32. I.Z. Kiss, W. Wang, and J.L Hudson, "Complexity of Globally Coupled Chaotic Electrochemical Oscillators," *Physical Chemistry Chemical Physics* 2, (2000): p. 3847-3854.
33. W. Wang, I. Z. Kiss, and J. L. Hudson, "Clustering of Arrays of Chaotic Chemical Oscillators by Feedback and Forcing," *Phys. Rev. Lett.* 86, 21, (2001): p. 4954-4957.
34. W. Wang, B.J. Green, and J. L. Hudson, "Periodic forcing of arrays of chaotic electrochemical oscillators," *J. Phys. Chem. B*. 105, 30, (2001): p. 7366-7373.
35. W. Wang, I. Z. Kiss, and J. L. Hudson, "Synchronization and clustering of arrays of electrochemical oscillators with global feedback," *Ind. Eng. Chem. Res.* 41, (2002): p. 330-339.
36. I.Z. Kiss, W. Wang, and J. L. Hudson, "Populations of coupled electrochemical oscillators," *Chaos* 12, 1, (2002): p. 252-263.
37. I. Z. Kiss, Y. Zhai, and John L. Hudson, "Collective dynamics of a weakly coupled electrochemical reaction on an array," *Ind. Eng. Chem. Res.* 41, (2002): p. 6363-6374.
38. Y. Zhai, I. Z. Kiss, and J. L. Hudson, "Emerging Coherence of Oscillating Chemical Reactions on Arrays: Experiments and Simulations," *Ind. Eng. Chem. Res.* 43, 2, (2004) p. 315-326.
39. Y. Zhai, I.Z. Kiss, and J. L. Hudson, "Amplitude Death through a Hopf Bifurcation in Coupled Electrochemical Oscillators: Experiments and Simulations," *Phys. Rev. E.* 69, 026208 (2004).

40. T.T. Lunt, V. Brusamarello, J.R. Scully, and J.L. Hudson, "Interactions among localized corrosion sites investigated with electrode arrays," *Proceedings - Electrochemical Society* (1999), 99-27(Passivity and Localized Corrosion), p. 414-424.
41. T.T. Lunt, V. Brusamarello, J. R. Scully, and J. L. Hudson, "Interactions Among Localized Corrosion Sites Investigated with Electrode Arrays," *Electrochemical and Solid State Letters* 3, 6, (2000): p. 271-274.
42. T.T. Lunt, J.R. Scully, V. Brusamarello, A.S. Mikhailov, and J.L. Hudson, "Spatial interactions among localized corrosion sites: experiments and modeling," *Proceedings - Electrochemical Society* (2001), 2000-25 (Pits and Pores II: Formation, Properties, and Significance for Advanced Materials), p. 115-125.
43. T.T. Lunt, J.R. Scully, V. Brusamarello, A.S. Mikhailov, and J.L. Hudson, "Spatial interactions among localized corrosion sites: experiments and modeling," *J. Electrochemical Soc.* 149, 5, B163-B173 (2002).
44. N. D. Budiansky and J.R. Scully, "Origins of persistent interaction among localized corrosion sites" *Proceedings - Electrochemical Society* (2003), 2002-24(Critical Factors in Localized Corrosion IV), 133-146.
45. N.D. Budiansky, J.L. Hudson, J.R. Scully, "Origins of Persistent Interaction among Localized Corrosion Sites on Stainless Steel" *Journal of the Electrochemical Society* (2004), 151(4), B233-B243].
46. D. Battocchi, J. He, G.P. Bierwagen a, D.E. Tallman, "Emulation and study of the corrosion behavior of Al alloy 2024-T3 using a wire beam electrode (WBE) in conjunction with scanning vibrating electrode technique (SVET)", *Corrosion Science* 47 (2005) 1165–1176}.
47. N. Missert, R.G. Copeland, F.D. Wall, C.M. Johnson, J.C. Barbour, P. Kotula, "Aluminum corrosion at systems of engineered copper particles" *Proceedings - Electrochemical Society* (2002), 2002-13(Corrosion Science), 307-313.
48. F.D. Wall, M.A. Martinez, C.M. Johnson, J.C. Barbour, N. Missert, R.G. Copeland, "Does anything pin the pitting behavior of aluminum?", *Proceedings - Electrochemical Society* (2004), 2003-23, 1-11].
49. F.D. Wall and M.A. Martinez, "Using microelectrodes to determine the availability and behavior of pit initiation sites in aluminum", *Proceedings - Electrochemical Society* (2001), 2000-23(Corrosion and Corrosion Prevention of Low Density Metals and Alloys), 229-238.
50. F.D. Wall, and M.A. Martinez, "A Statistics-Based Approach to Studying Aluminum Pit Initiation — Intrinsic and Defect-Driven Pit Initiation Phenomena", *Journal of the Electrochemical Society*, 2003. 150(4): p. B146-B157.
51. F.D. Wall, C. M. Johnson, J. C. Barbour, and M. A. Martinez, "The Effects of Chloride Implantation on Pit Initiation in Aluminum" *Journal of The Electrochemical Society*, 151(2), B77-B81 ,2004.

52. F.D. Wall, M.A. Martinez, and J.J. Van den Avyle, "Relationship between Induction Time for Pitting and Pitting Potential for High-Purity Aluminum", *Journal of the Electrochemical Society*, 2004. 151(6): p. B354-8.
53. W. Zhang, B. Hurley, R.G. Buchheit, "Characterization of Chromate Conversion Coating Formation and Breakdown Using Electrode Arrays *Journal of the Electrochemical Society* (2002), 149(8), B357-B365].
54. F. D. Wall and M. A. Martinez, "The Effect of Electrode Thickness and Interelectrode Spacing on Electrochemical Signals at Low Humidity" Abs. 480, 204th Meeting, The Electrochemical Society, Inc.(2004).
55. Y.J. Tan, "Studying non-uniform electrodeposition using the wire beam electrode method", *International Journal of Modern Physics B (World Scientific)*, no.1&2 - special issue for proceedings of International Conference on Materials for Advanced Technologies, Singapore (1-6 July 2001), vol.16, pp144-150(2002).
56. Y.J. Tan and K.Y. Lim, "Characterising Nonuniform Electrodeposition and Electrodeposition Using the Novel Wire Beam Electrode Method", *Journal of Applied Electrochemistry*, vol.34, pp1093-1101(2004).
57. Y.J. Tan, "Wire Beam Electrode: A New Tool for Localized Corrosion Studies" *Proceedings of Australasian Corrosion Association Corrosion & Prevention 97*, Paper No. 52, Australasian Corrosion Association, Australia., Nov. 9-12, 1997.
58. Y.J. Tan, "Monitoring Localized Corrosion Processes and Estimating Localized Corrosion Rates Using a Wire-beam Electrode", *Corrosion*, Vol 54 (No.5), 1998, p403-413.
59. H. Eren, A. Lowe, Y.J. Tan, S. Bailey, and B. Kinsella, "An auto-switch for multi-sampling of a wire beam electrode corrosion monitoring system", *IEEE Transaction on Instrumentation and Measurement*, vol.47, p1096-2001 (1998).
60. Y.J. Tan, "Wire Beam Electrode: A New Tool for Studying Localized Corrosion and Other Inhomogeneity Electrochemical Processes" *Corrosion Science*, Vol 41 (No.2), 1999, 229-247.
61. Y.J. Tan, S. Bailey, B. Kinsella, and A. Lowe, "Mapping corrosion kinetics using the wire beam electrode in conjunction with electrochemical noise resistance measurements", *Journal of the Electrochemical Society*, vol.147, no.2, p530-540 (2000).
62. Y. J. Tan, "Method and apparatus for measuring localized corrosion and other heterogeneous electrochemical processes", *United States of America Patent No. 6132593*, 24pp (2000).
63. Y.J. Tan, S. Bailey and B. Kinsella, "Mapping non-uniform corrosion in practical corrosive environments using the wire beam electrode method (I) - Multi-phase corrosion", *Corrosion Science*, vol.43, p1905 – 1918 (2001).
64. Y.J. Tan, S. Bailey and B. Kinsella, "Mapping non-uniform corrosion in practical corrosive environments using the wire beam electrode method (II) - Crevice corrosion" *Corrosion Science*, vol.43, p1919 – 1929(2001).

65. Y.J. Tan, S. Bailey and B. Kinsella, "Mapping non-uniform corrosion in practical corrosive environments using the wire beam electrode method (III) - Water-line corrosion", *Corrosion Science*, vol.43, p1930 – 1937 (2001).
66. Y. J. Tan, "Measuring Localized Corrosion Using the Wire Beam Electrode Method', in special Electrochemical Society publication: 'Corrosion Science: A Retrospective and Current Status', the Electrochemical Society 201st Meeting, Philadelphia, USA, pp. 377-384 (2002).
67. N. N. Aung, Y.J. Tan, "A New Method of Studying Buried Steel Corrosion and Its Inhibition Using the Wire Beam Electrode", *Corrosion Science*: 46, (2004), pp.3057-3067.
68. Y. J. Tan, "An experimental comparison of three wire beam electrode based methods for determining corrosion rates and patterns", *Corrosion Science*, 47 (2005) 1653–1665.
69. L. Yang, N. Sridhar, and O. Pensado, "Development of a Multielectrode Array Sensor for Monitoring Localized Corrosion", Presented at the 199th Meeting of the Electrochemical Society, Abstract #182, Extended Abstract Volume I, 2001.
70. L. Yang, N. Sridhar, O. Pensado and D. Dunn "An In-situ Galvanically Coupled Multi-Electrode Array Sensor for Localized Corrosion", *Corrosion*, 58, 1004, 2002.
71. L. Yang, and D. Dunn, "Evaluation of Corrosion Inhibitors in Cooling Water Systems Using a Coupled Multielectrode Array Sensor", *Corrosion/2002*, Paper No. 004, NACE International, 2002.
72. L. Yang, N. Sridhar, and G. Cragnolino, "Comparison of Localized Corrosion of Fe-Ni-Cr-Mo Alloys in Concentrated Brine Solutions Using a Coupled Multielectrode Array Sensor", *NACE Corrosion/2002*, Paper No. 545, NACE International, 2002.
73. C.S. Brossia, L. Yang, D.S. Dunn, N. Sridhar, "Corrosion Sensing and Monitoring" Proceedings of the Tri-Service Corrosion Conference, Jan. 14-18, 2002, San Antonio, TX, USA.
74. L. Yang and N. Sridhar, "Monitoring of Localized Corrosion", in *ASM Handbook, Volume 13A-Corrosion: Fundamentals, Testing, and Protection*, Stephen. D. Crammer and Bernard S. Covino, Jr., eds, ASM International, Materials Park, Ohio, pp. 519-524, 2003.
75. L. Yang and N. Sridhar "Coupled Multielectrode Online Corrosion Sensor", *Materials Performance*, Vol. 42, No.9, pp. 48-52, 2003.
76. L. Yang, R. T. Pabalan, L. Browning, and G. A. Cragnolino, "Measurement of Corrosion in Saturated Solutions under Salt Deposits Using Coupled Multielectrode Array Sensors", *CORROSION/2003*, paper no. 03426, (Houston, TX: NACE International, 2003).
77. L. Yang, R. T. Pabalan, L. Browning and D.S. Dunn, "Corrosion Behavior of Carbon Steel and Stainless Steel Materials under Salt Deposits in Simulated Dry Repository Environments", in *Scientific Basis for Nuclear Waste Management XXVI*, R. J. Finch and D. B. Bullen, eds, Warrendale, PA: Materials Research Society, M.R.S. Symposium Proceedings, Vol. 757, pp.791-797, 2003.

78. C. S. Brossia and L. Yang, "Studies of Microbiologically Influenced Corrosion Using a Coupled Multielectrode Array Sensor", CORROSION/2003, paper no. 03575, (Houston, TX: NACE International, 2003).
79. A. Anderko, N. Sridhar, C. S. Brossia, D. S. Dunn, L.T. Yang, B.J. Saldanha, S.L. Grise, and M.H. Dorsey, "An Electrochemical Approach to Predicting and Monitoring Localized Corrosion in Chemical Process Streams", CORROSION/2003, paper no. 03375, (Houston, TX: NACE International, 2003).
80. V. Jain, S. Brossia, D. Dunn, and L. Yang, "Development of Sensors for Waste Package Testing and Monitoring in the Long Term Repository Environments", Ceramic Transactions, Vol. 143, pp. 283-290, 2003, American Ceramic Society, Westerville, OH.
81. L. Yang, R.T. Pabalan and D.S. Dunn, "The Study of Atmospheric Corrosion of Carbon Steel and Aluminum under Salt Deposit Using Coupled Multielectrode Array Sensors", Presented at the 204th Meeting of the Electrochemical Society, Abstract #465, Extended Abstract Volume 2003-II.
82. L. Yang and N. Sridhar, "Sensor array for electrochemical corrosion monitoring", US patent 6,683,463 (2004).
83. L. Yang and N. Sridhar, S.L. Grise, B. J. Saldanha, M.H. Dorsey, H. J. Shore and A. Smith, "Real-Time Corrosion Monitoring in a Process Stream of a Chemical Plant Using Coupled Multielectrode Array Sensors", CORROSION/2004, paper no. 04440, Houston, TX: NACE International, 2004.
84. L. Yang, N. Sridhar, D. S. Dunn and C. S. Brossia, Laboratory Comparison of Coupled Multielectrode Array Sensors with Electrochemical Noise Sensors for Real-time Corrosion Monitoring, CORROSION/2004, paper no. 04429, Houston, TX: NACE International, 2004.
85. L. Yang and G.A. Cragolino, "Studies on The Corrosion Behavior of Stainless Steels in Chloride Solutions in the Presence of Sulfate Reducing Bacteria", CORROSION/2004, paper no. 04598, Houston, TX: NACE International, 2004.
86. M.H. Dorsey, L. Yang and N. Sridhar, "Cooling Water Monitoring Using Coupled Multielectrode Array Sensors and Other On-line Tools", CORROSION/2004, paper no. 04077, Houston, TX: NACE International, 2004.
87. L. Yang, N. Sridhar, C. S. Brossia and D. S. Dunn, "Evaluation of the Coupled Multielectrode Array Sensor as a Real Time Corrosion Monitor", Corrosion Science, Vol 47, pp.-1794-1809 (2005).
88. A. Anderko, N. Sridhar¹ and L. Yang, S.L. Grise, B.J. Saldanha, and M.H. Dorsey, "Validation of a Localized Corrosion Model Using Real-Time Corrosion Monitoring in a Chemical Plant", Corrosion Engineering, Science and Technology (formerly British corrosion J.), Vol 40, pp.33-42, August, 2005.

89. L. Yang, D. Dun and G. Cragnolino, "An Improved Method for Real-time and Online Corrosion Monitoring Using Coupled Multielectrode Array Sensors", CORROSION/2005, paper no. 05379, (Houston, TX: NACE International, 2005).
90. L. Yang, D. Dun, Y.-M. Pan and N. Sridhar, "Real-time Monitoring of Carbon Steel Corrosion in Crude Oil and Brine Mixtures Using Coupled Multielectrode Sensors" CORROSION/2005, paper no. 05293, (Houston, TX: NACE International, 2005).
91. M. H. Dorsey, D. R. Demarco, B. J. Saldanha, G. A. Fisher, L. Yang and N. Sridhar, "Laboratory Evaluation of a Multi-Array Sensor for Detection of Underdeposit Corrosion and/or Microbially Influenced Corrosion", CORROSION/2005, paper no. 05371 (Houston, TX: NACE, 2005).
92. X. Sun and L. Yang, "Real-time Measurement of Crevice Corrosion with Coupled Multielectrode Array Sensors", CORROSION/2006, paper no. 06679 (Houston, TX: NACE, 2006).
93. X. Sun and L. Yang, "Real-Time Monitoring of Localized and General Corrosion Rates in Simulated Marine Environments Using Coupled Multielectrode Array Sensors", CORROSION/2006, paper no. 06284 (Houston, TX: NACE, 2006).
94. X. Sun and L. Yang, "Real-Time Monitoring of Localized and General Corrosion Rates in Drinking Water Utilizing Coupled Multielectrode Array Sensors", CORROSION/2006, paper no. 06094 (Houston, TX: NACE, 2006).
95. K. Chiang and L. Yang, "Monitoring Corrosion Behavior of a Cu-Cr-Nb Alloy by Multielectrode Sensors", CORROSION/2006, paper no. 06676 (Houston, TX: NACE, 2006).
96. N. Sridhar, L. Yang and F. Song, "Application of Multielectrode Array to Study Dewpoint Corrosion in High Pressure Natural Gas Pipeline Environments", CORROSION/2006, paper no. 06673 (Houston, TX: NACE, 2006).
97. X. Sun "Online Monitoring of Undercoating Corrosions Utilizing Coupled Multielectrode Sensors", CORROSION/2004, paper no. 04033, (Houston, TX: NACE International, 2004).
98. X. Sun, "Online Monitoring of Corrosion under Cathodic Protection Conditions Utilizing Coupled Multielectrode Sensors", CORROSION/2004, paper no. 04094, Houston, TX: NACE International, 2004).
99. X. Sun, "Online and Real-Time Monitoring of Carbon Steel Corrosion in Concrete, Using Coupled Multielectrode Sensors", CORROSION/2005, paper no.05267 (Houston, TX: NACE, 2005).
100. X. Sun, "Real-Time Corrosion Monitoring in Soil with Coupled Multielectrode Sensors" CORROSION/2005, paper no.05381 (Houston, TX: NACE, 2005).
101. X. Sun, "Online Monitoring of Undercoating Corrosion Using Coupled Multielectrode Sensors", Materials Performance, 44(2), p28-32 (2005).

102. P. Angell, "Use of the Multiple-Array-Sensor to Determine the Effect of Environmental Parameters on Microbial Activity and Corrosion Rates". CORROSION/2006, paper no. 06671 (Houston, TX: NACE, 2006).

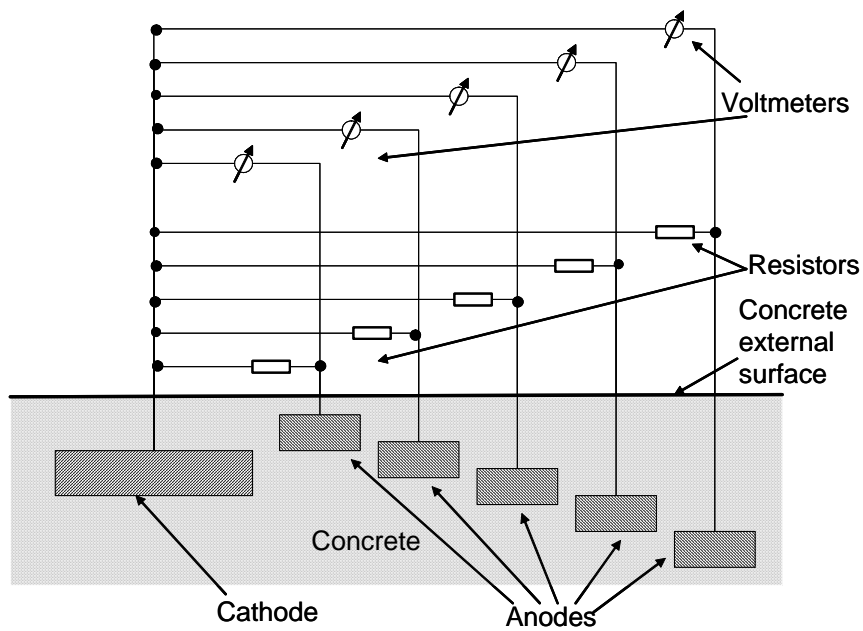


Figure 1. Schematic diagram of a galvanically coupled multielectrode system used to detect the onset of corrosion of carbon steel reinforcing materials at different locations. Note: The anodes were made of carbon steels similar to the reinforcing material; the cathode was made of special steels or alloys. Source: Ref. 1.

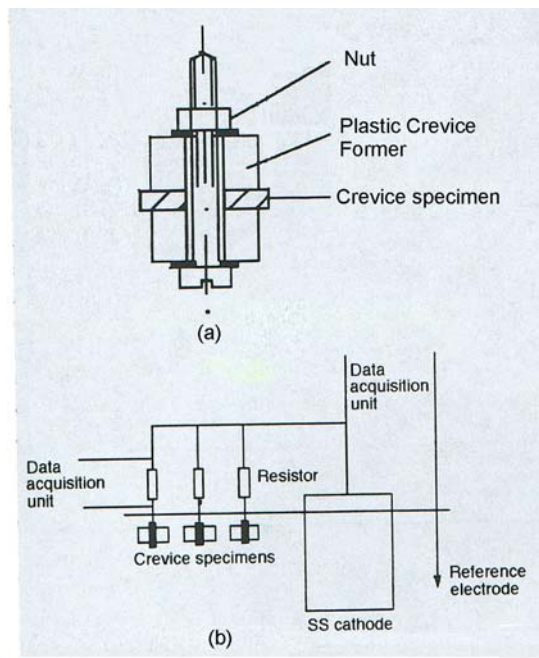


Figure 2. Schematic diagram of a galvanically coupled crevice cell system. (a) crevice assembly and (b) galvanic coupling of crevice assemblies and stainless cathode. Source: Ref. 11.

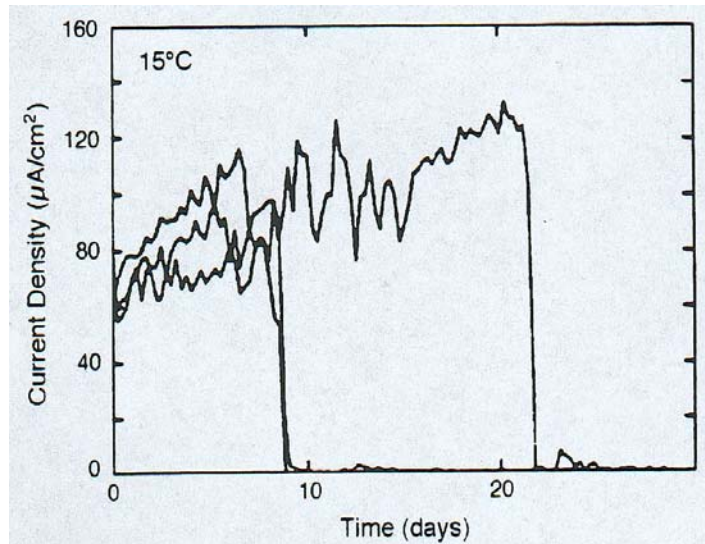


Figure 3. Galvanic current densities between three creviced specimens of welded UNS S31254 and a cathode as a function of time in seawater at 15°C. Source: Ref. 11.

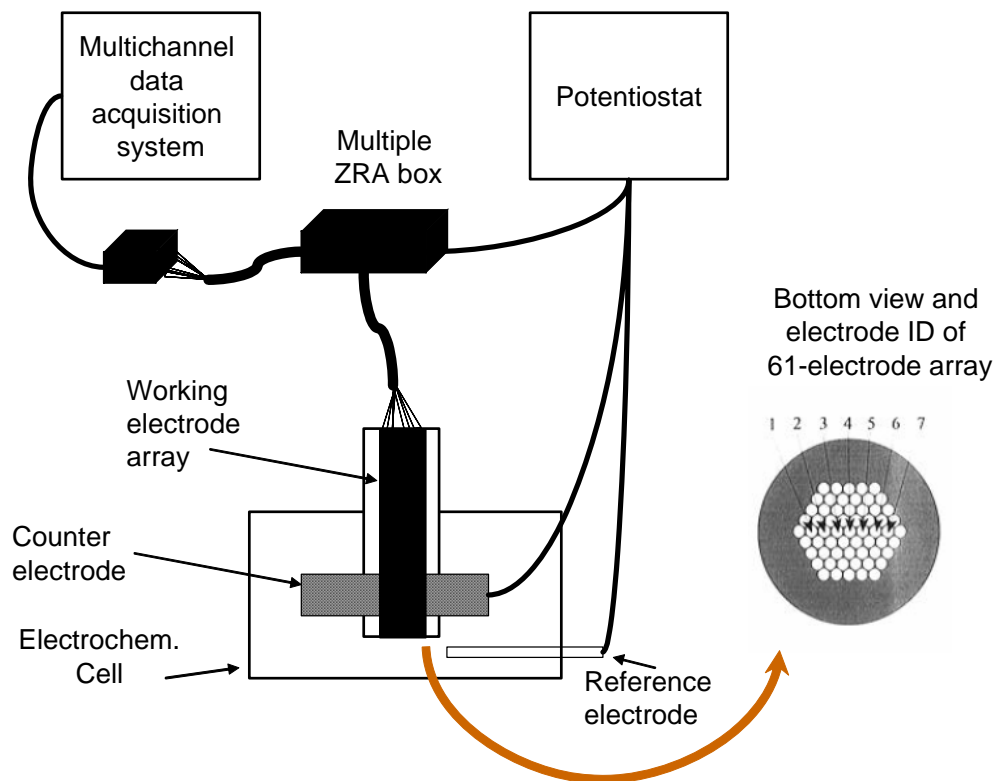


Figure 4. Schematic diagram of a coupled multi-electrode array system used to study the spatiotemporal pattern of the nonuniform corrosion of iron in sulfuric acid solution. Modified according to Ref. 24, with permission from Z. Fei and J.L. Hudson.

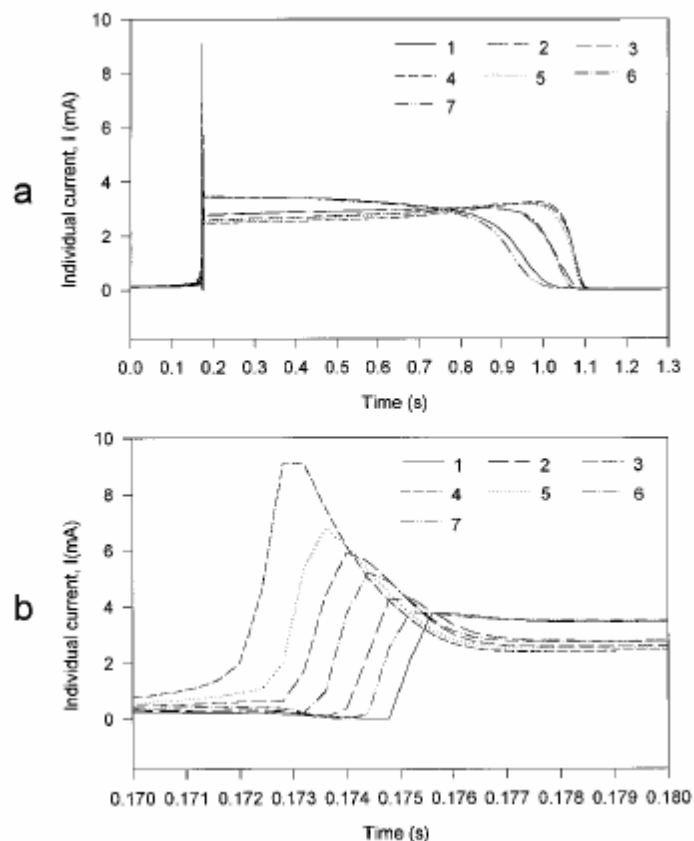


Figure 5. Currents of individual electrodes on the 61-electrode array, as shown in Figure 4, during (a) activation and (b) passivation. Note: The electrode numbers are shown in Figure 4. Source: Ref. 25, with permission from American Chemical Society.

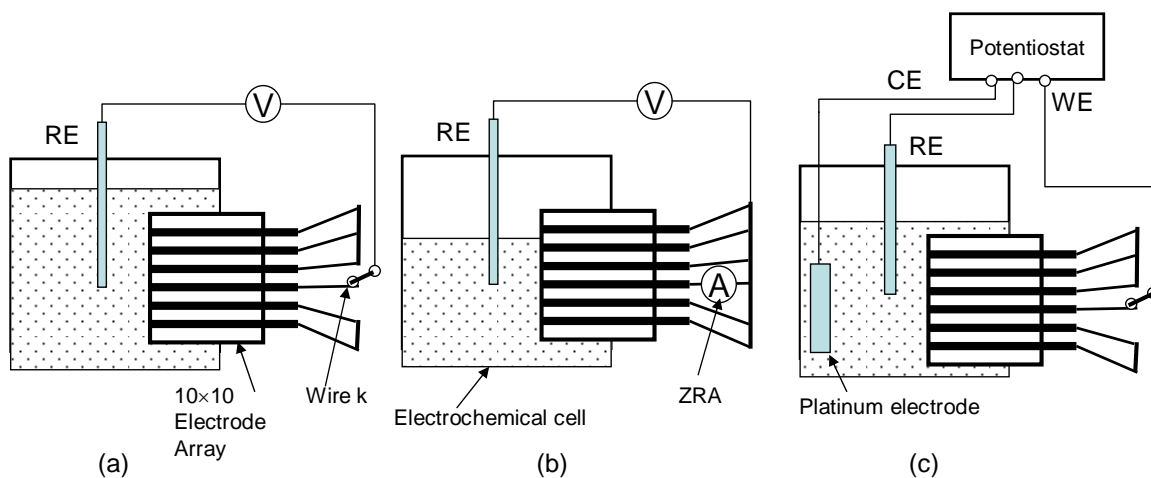


Figure 6. Schematic diagram of the coupled multielectrode array system for measurement of (a) open-circuit potentials of individual wires, (b) galvanic currents between individual wires and the system and (c) Tafel slopes of individual wires. Source: Ref. 58.

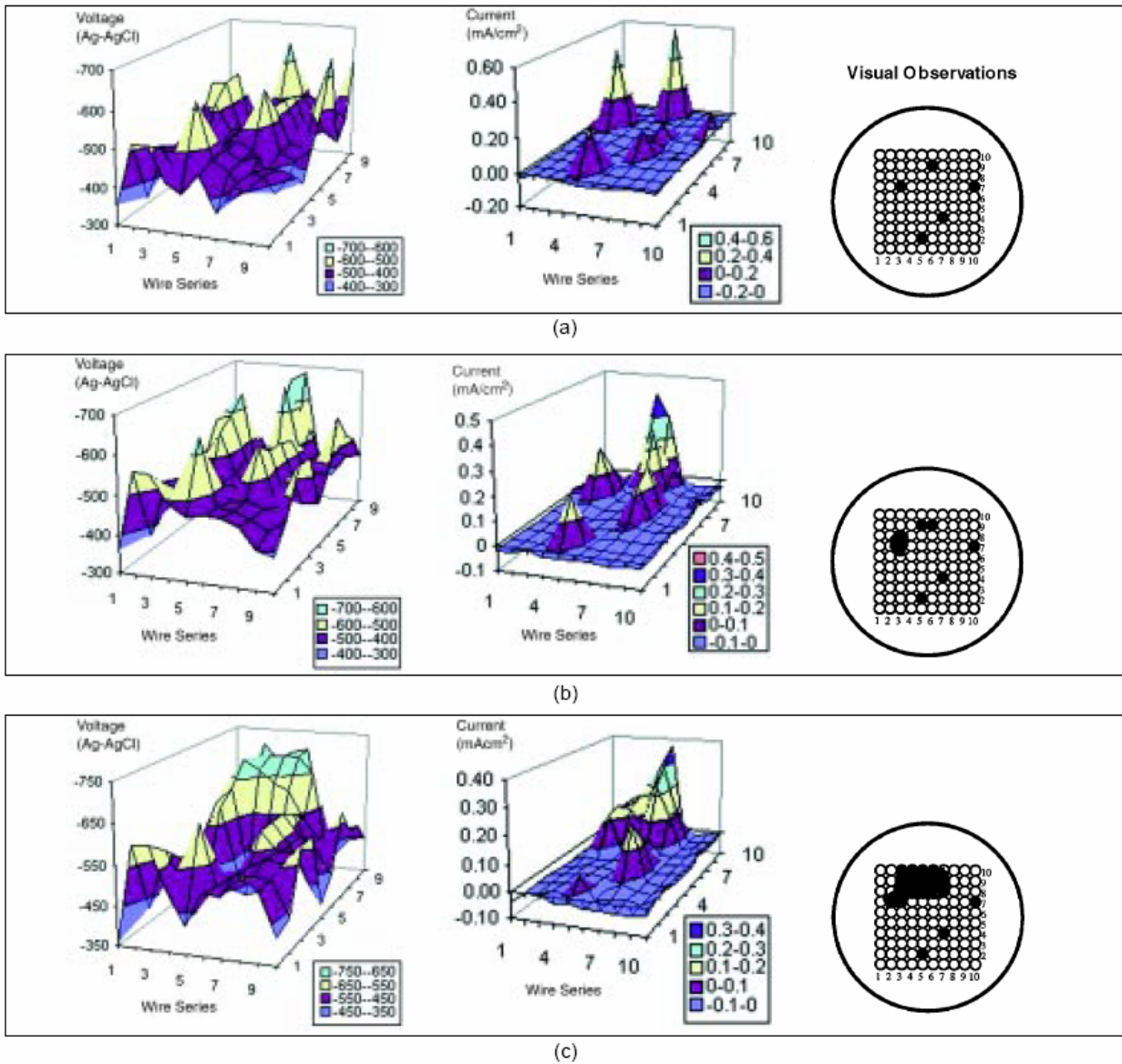


Figure 7. Visual observations of electrodes, and potential and galvanic current distributions over the 10×10 array surface of carbon steel during exposure to 0.017 M NaCl + 0.008 M Na₂CO₃ solution after (a) 1-h exposure, (b) 4-h exposure, and (c) 24-h exposure. Source: Ref. 58.

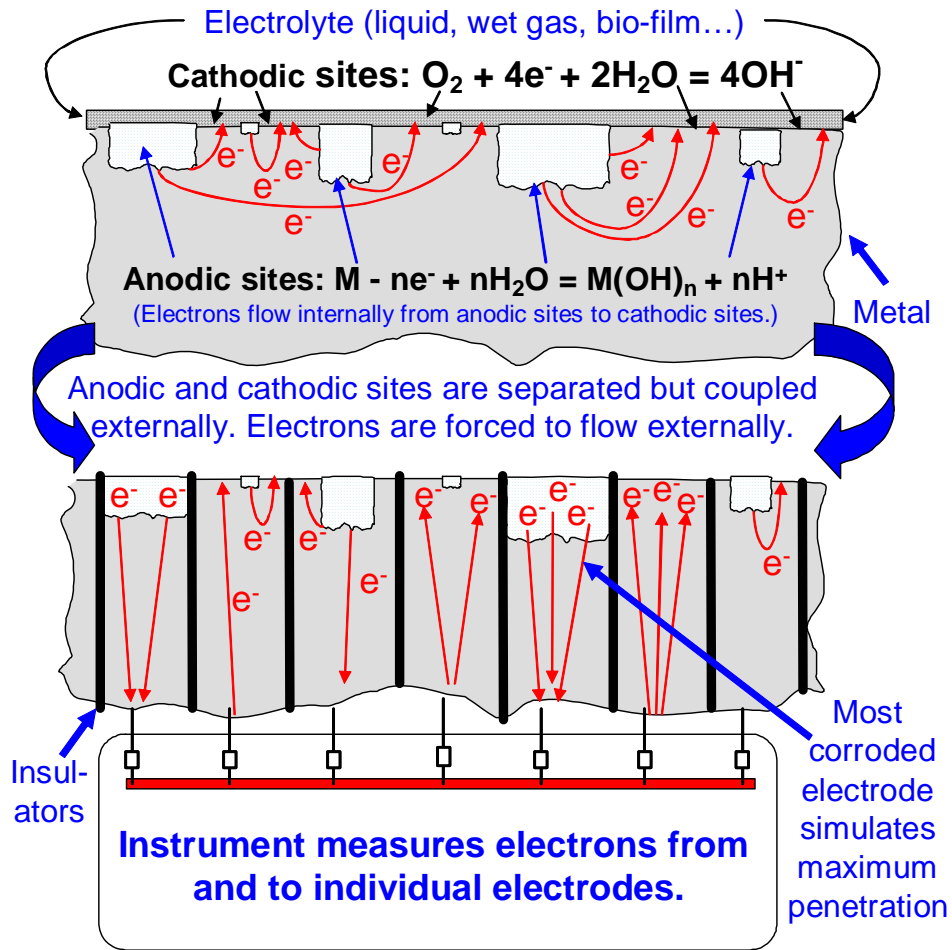


Figure 8. Schematic diagram showing the principle of coupled multi-electrode array sensors for localized corrosion monitoring. Source: Ref. 94.



Figure 9. Typical coupled multi-electrode sensor probes for applications in corrosion monitoring and electrochemical studies. Source: Ref. 75 and Ref. 93.

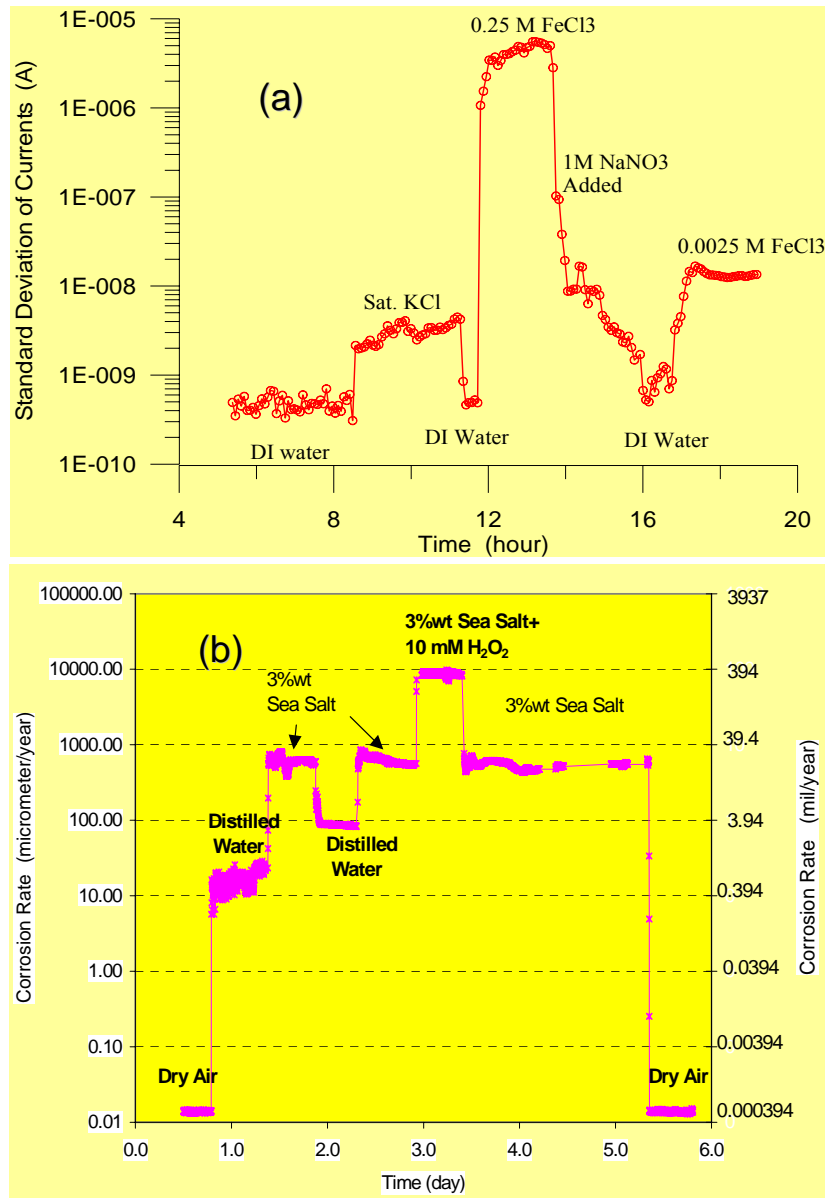


Figure 10. Typical response of standard deviation of the current signals from (a) a 25-electrode type 304 stainless steel probe and (b) a 16-electrode carbon steel probe to the changes in solution chemistry. Source: Ref. 78 and Ref. 98.

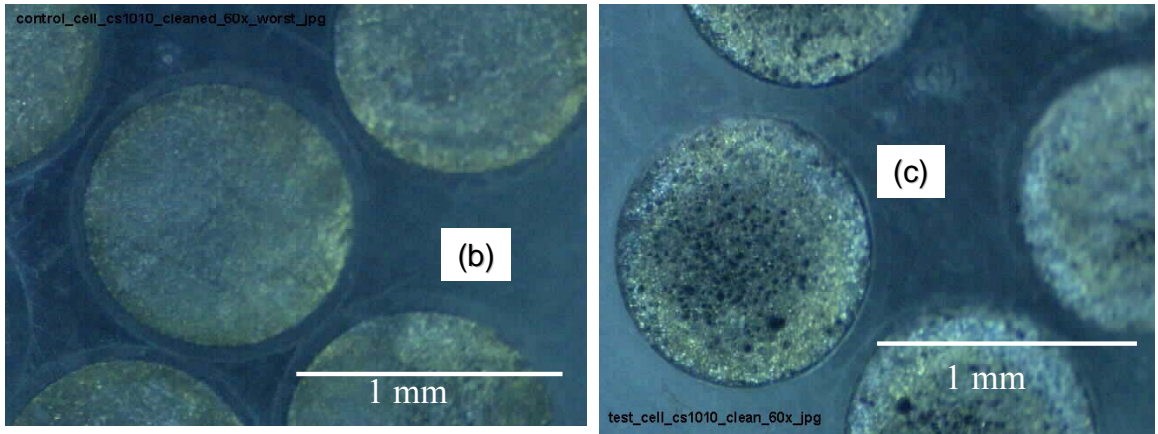
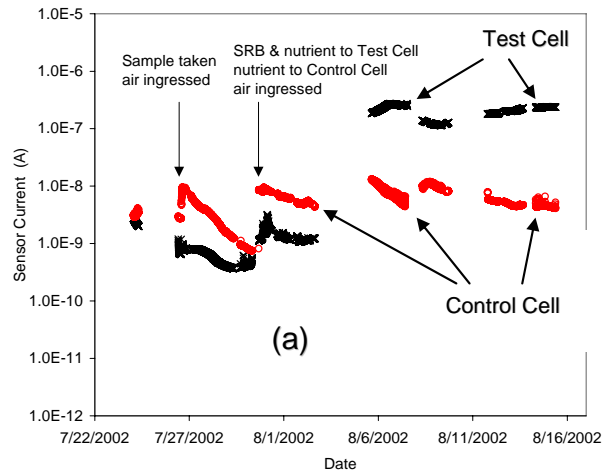


Figure 11. (a) Typical responses of carbon steel CMAS probes in biotic (SRB) and abiotic NaCl solutions, and post test appearances of the probes after exposure to (b) abiotic solution and (c) biotic solution. Source: Ref. 73.

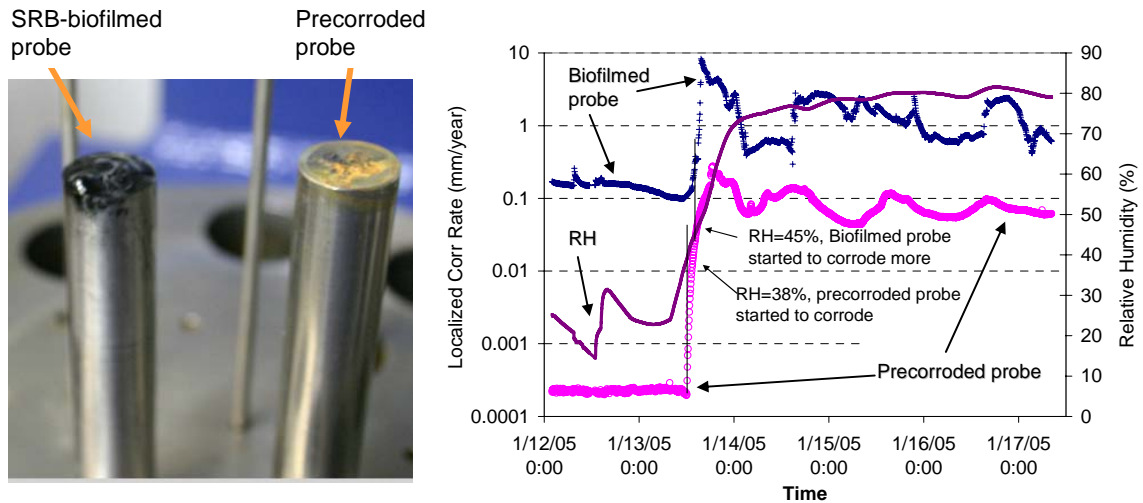


Figure 12. Experimental setup and results for the evaluation of localized corrosion for carbon steel under biofilm at different relative humidities in a simulated high-pressure natural gas system. Note: The sulfate-reducing bacteria (SRB) deposits were formed in a slime former; the sensing surface of the precorroded probe was covered by corrosion products formed in an H₂S-containing water. Source: Ref. 96.

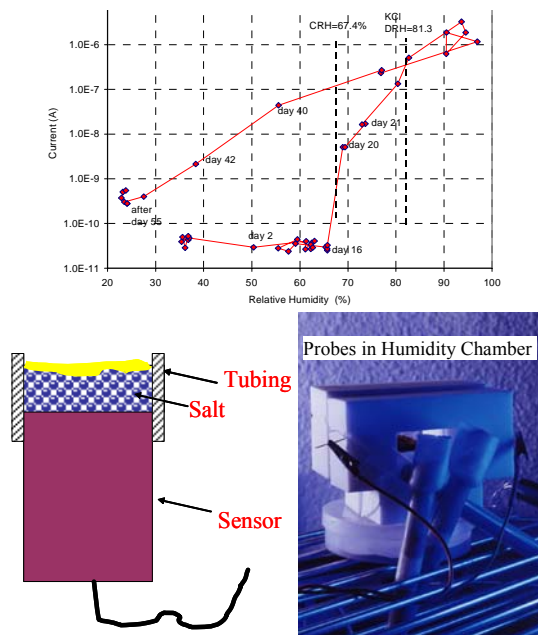


Figure 13. Experimental setup and the results for the evaluation of localized corrosion of carbon steel using CMAS probes under salt deposits (initially pure KCl powder) at different relative humidities in air. Source: Ref. 77.

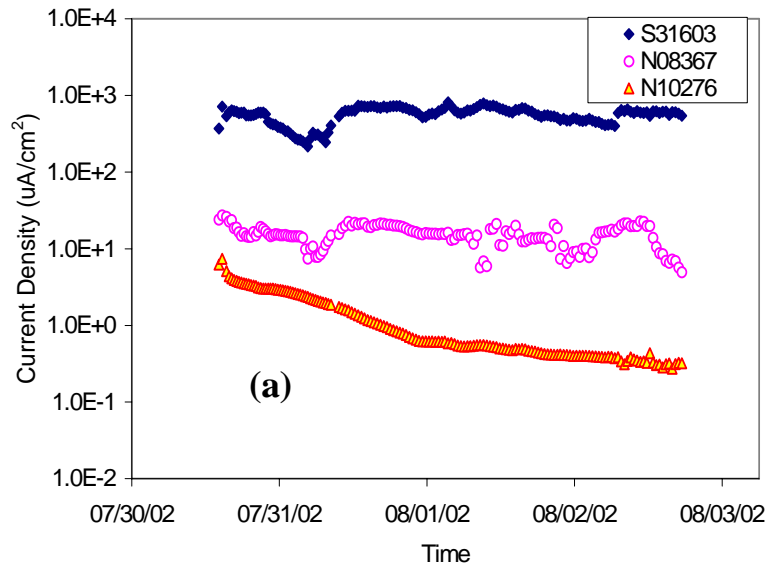


Figure 14. (a) Maximum localized corrosion currents of three alloys in (b) a pressurized stream of a chemical plant at elevated temperatures. Source: Ref. 79 and Ref. 83.

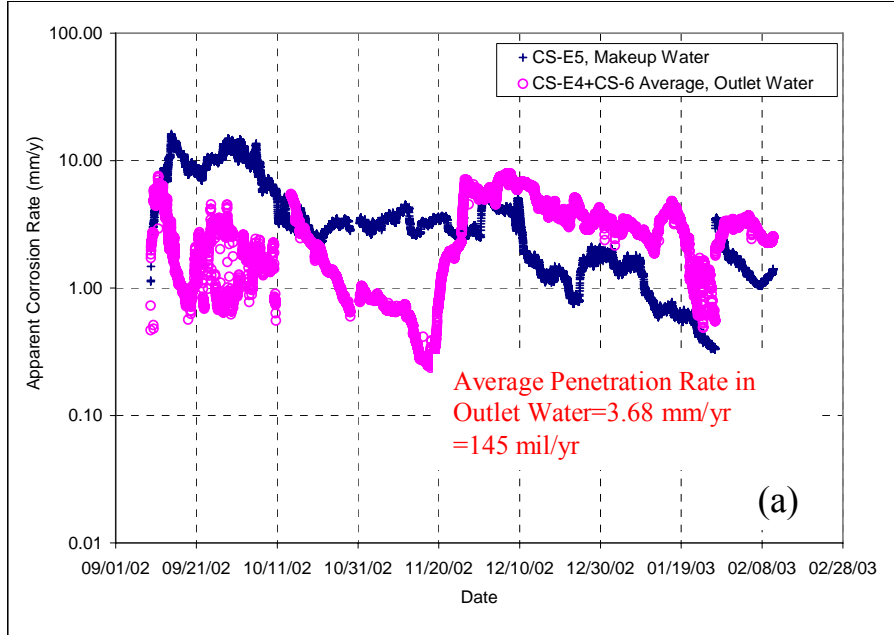


Figure 15. (a) Typical maximum localized corrosion rates of CMAS carbon steel probes measured in (b) a cooling water monitoring station of a chemical plant. Source: Ref. 86.



Coupon tests showed 100 to 200 mil/yr (2.5 to 5 mm/yr) pitting rate



Before cleaning



After cleaning

Figure 16. Comparison of the post test appearances of the CMAS carbon steel probes and the coupon test specimens in the cooling water system of a chemical plant.
Source: Ref. 86.

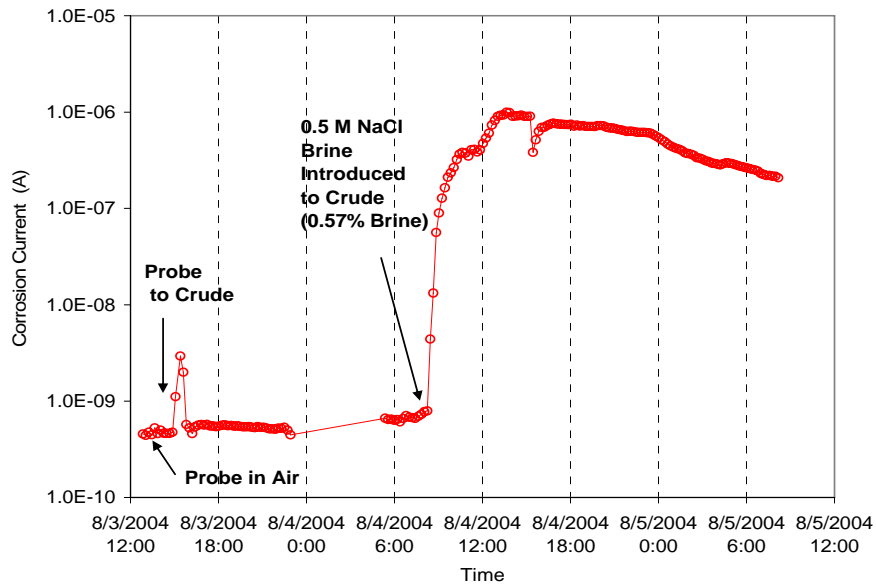


Figure 17. Typical responses of a carbon steel CMAS probe to the addition of brine in crude oil. Source: Ref. 90.

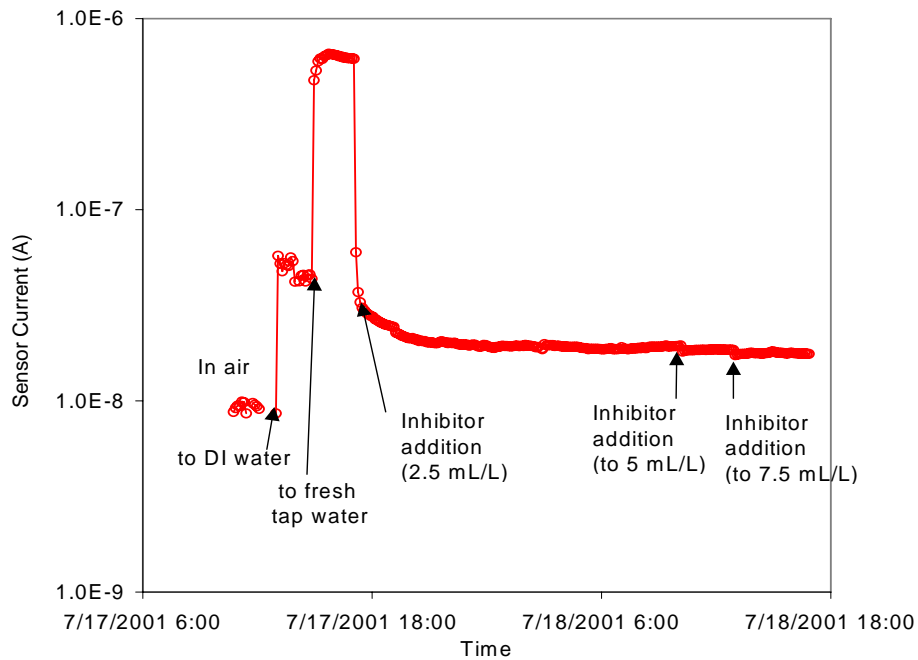


Figure 18. Typical responses of the current signal from a carbon steel CMAS probe to the dosing of a commercial corrosion inhibitor. Source: Ref. 71.

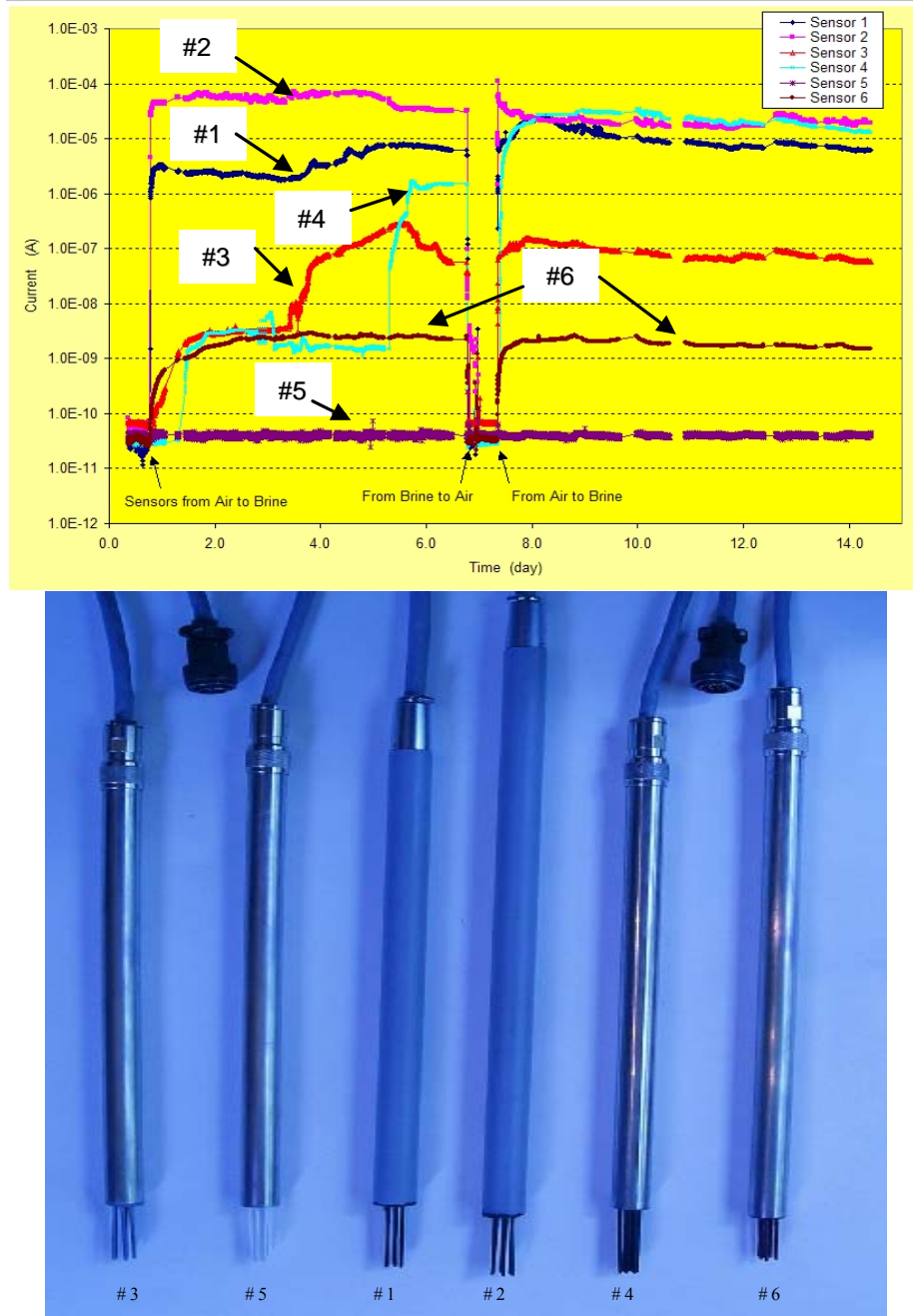


Figure 19. The corrosion currents (top figure) measured from carbon steel CMAS probes (bottom figure) whose sensing electrodes were coated with different types of commercial paints. Note: The electrodes of the CMAS probe were finger type. The coatings on the electrode of Probes #1 and #2 had initial mechanically induced defects. Source: Ref. 97.

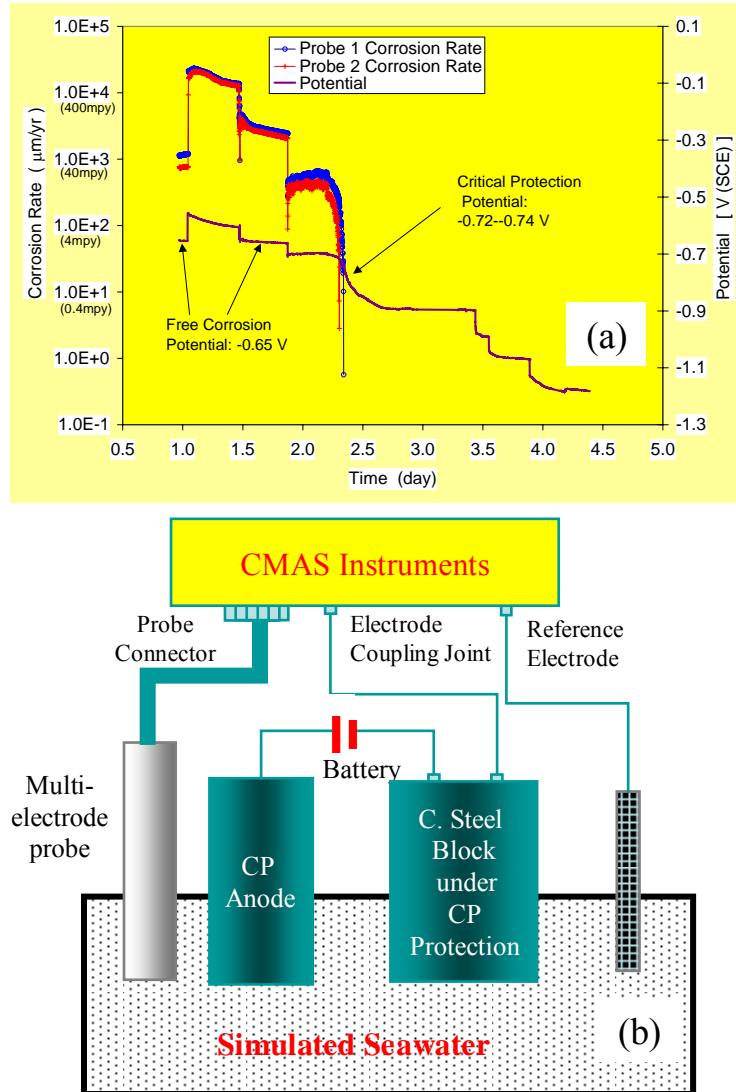


Figure 20. (a) Responses of the maximum localized corrosion rates measured from two carbon steel probes and (b) the connections of a typical probe to a CMAS instrument under cathodic protection conditions. Source: Ref. 98 and Ref. 99.

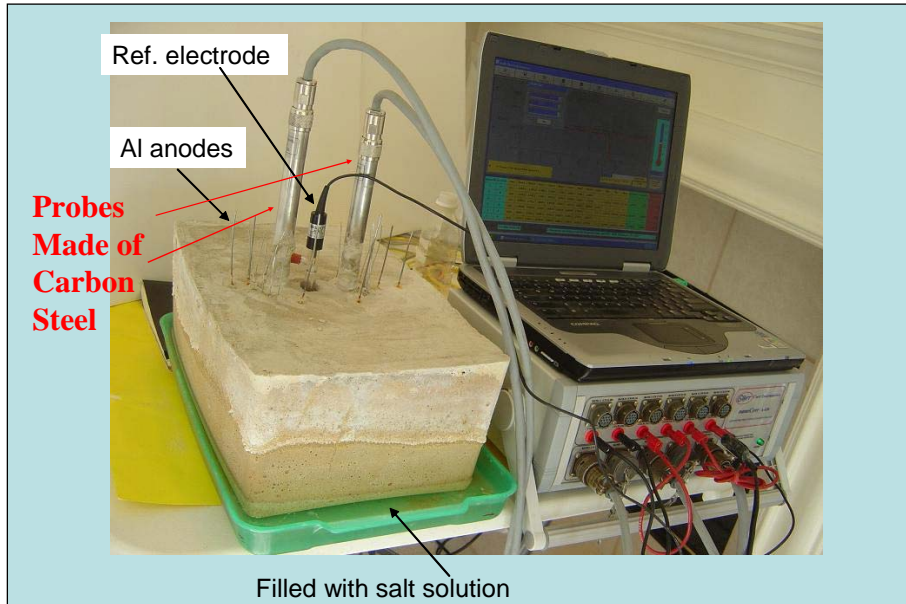


Figure 21. Experimental setup for localized corrosion measurements in concrete using carbon steel CMAS probes. Note: The aluminum anodes were used for testing the effectiveness of cathodic protection. Source: Ref. 99.

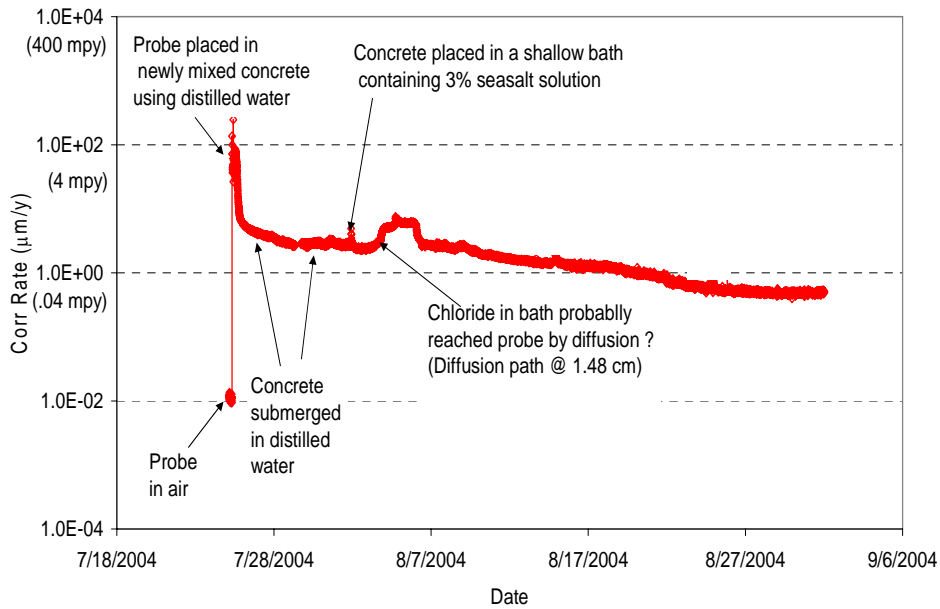


Figure 22. Response of the maximum localized corrosion rate measured from a carbon steel CMAS probe in concrete that was initially immersed in distilled water and then in simulated seawater. Note: The sensing surface of the probe was 1.48 cm from the concrete bottom surface. The increase in corrosion rate two days after the immersion in simulated seawater was probably due to the arrival of chloride to the probe by diffusion. Source: Ref. 99.

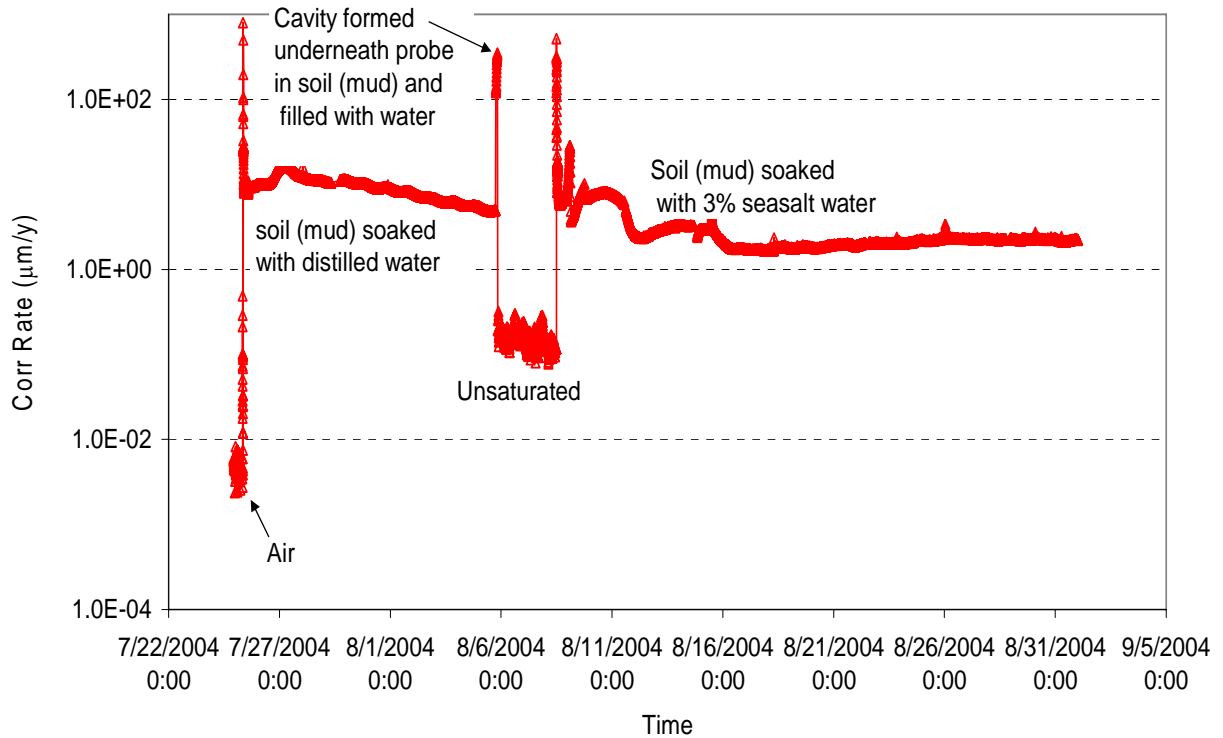


Figure 23. Maximum localized corrosion rates measured from a carbon steel CMAS probe in air, in soil soaked with distilled water, in soil cavity filled with water, in soil above water line (unsaturated with water), and in densely packed soil soaked with 3% seasalt water. Source: Ref. 100.

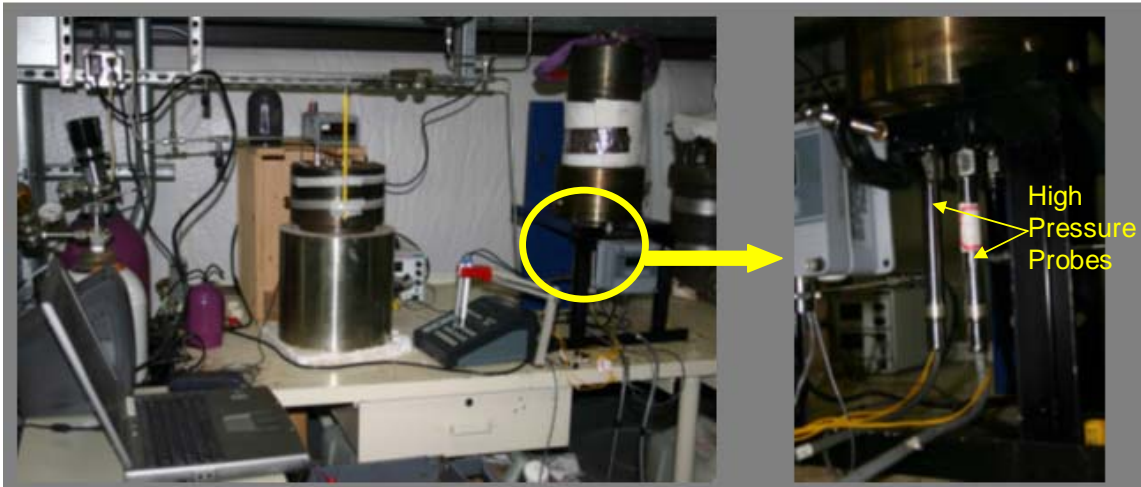
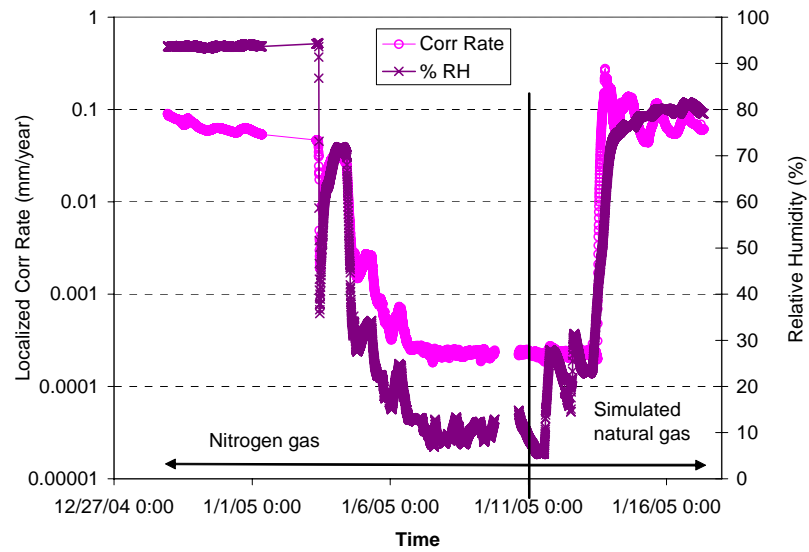


Figure 24. Experimental setup (bottom) and the results (top) from a carbon steel CMAS probe at different relative humidities in a high pressure system. Source: Ref. 96.

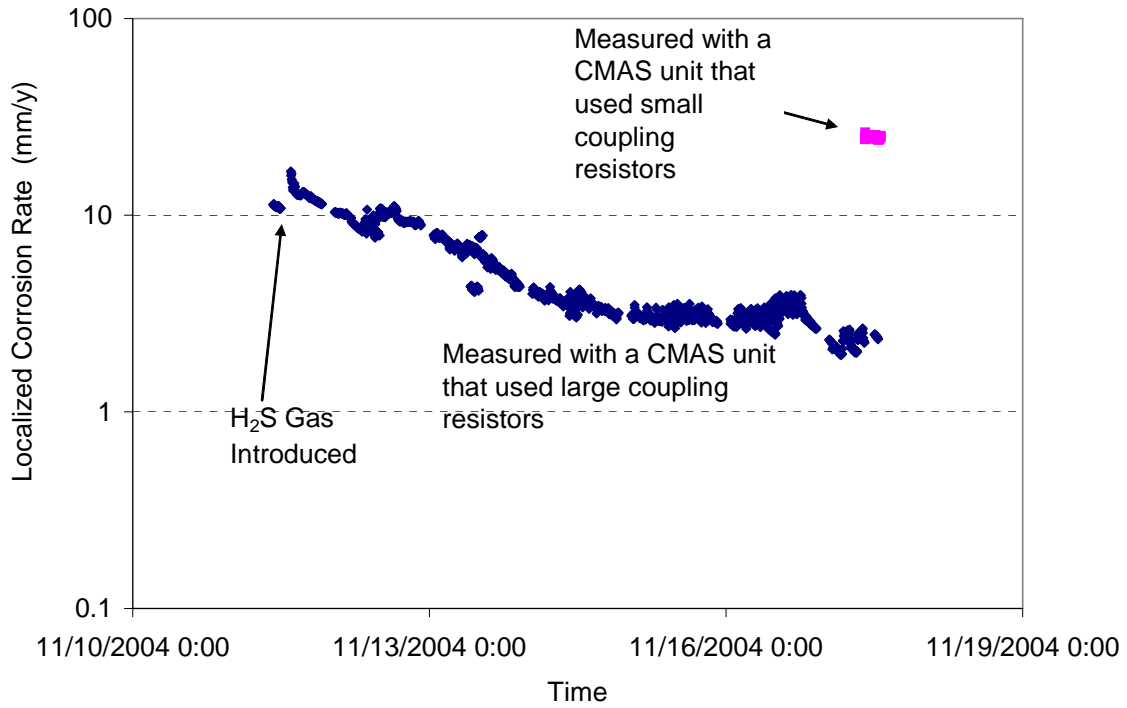


Figure 25. Maximum localized corrosion rate measured from a carbon steel CMAS probe in a solution saturated with pure H₂S at ambient temperature and pressure using two CMAS instrument units. Source: Ref. 96.

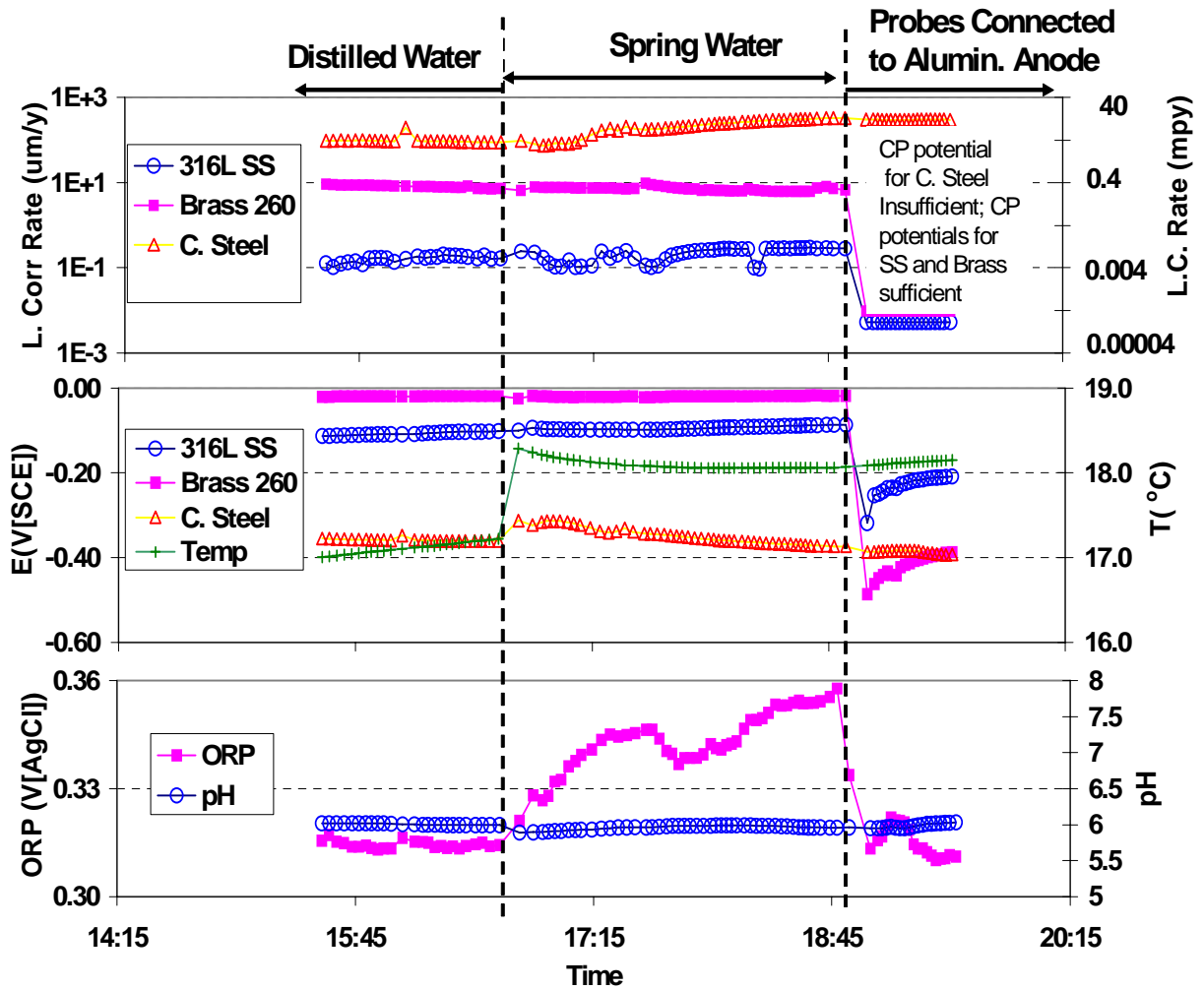


Figure 26. Maximum localized corrosion rates and potentials measured from Type 316L stainless steel, Type 260 brass, and Type 1008 carbon steel CMAS probes in water, temperature, pH, and ORP of the water during a short-term testing with and without cathodic protection. Note: Probe electrodes were connected to aluminum anodes for cathodic protection. Source: Ref. 94.

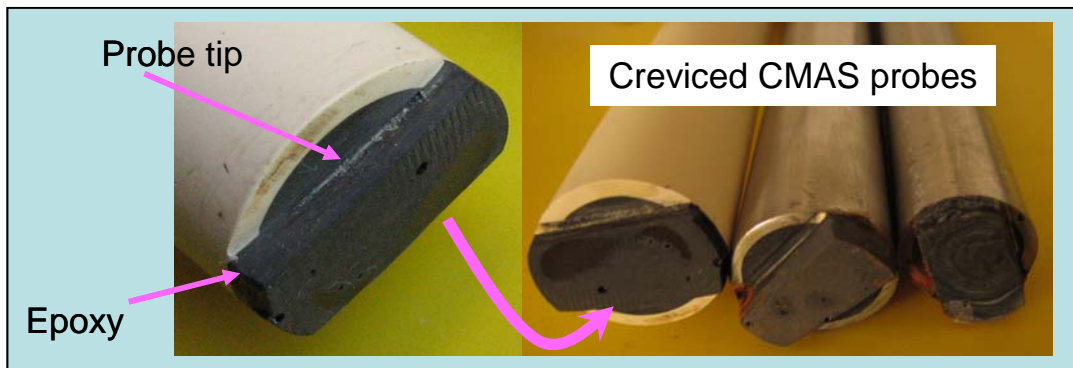
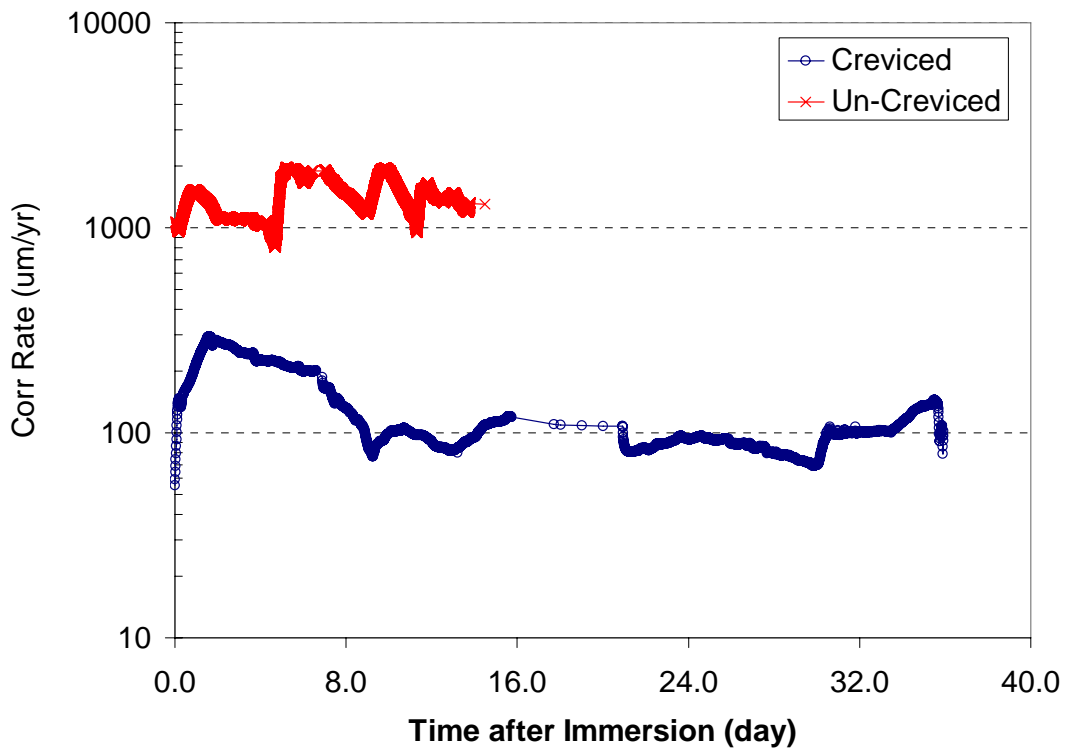


Figure 27. Typical creviced CMAS probes and the maximum localized corrosion rates measured from a creviced probe and an uncreviced probe, respectively, for Type 1008 carbon steel in simulated seawater. Source: Ref. 92.

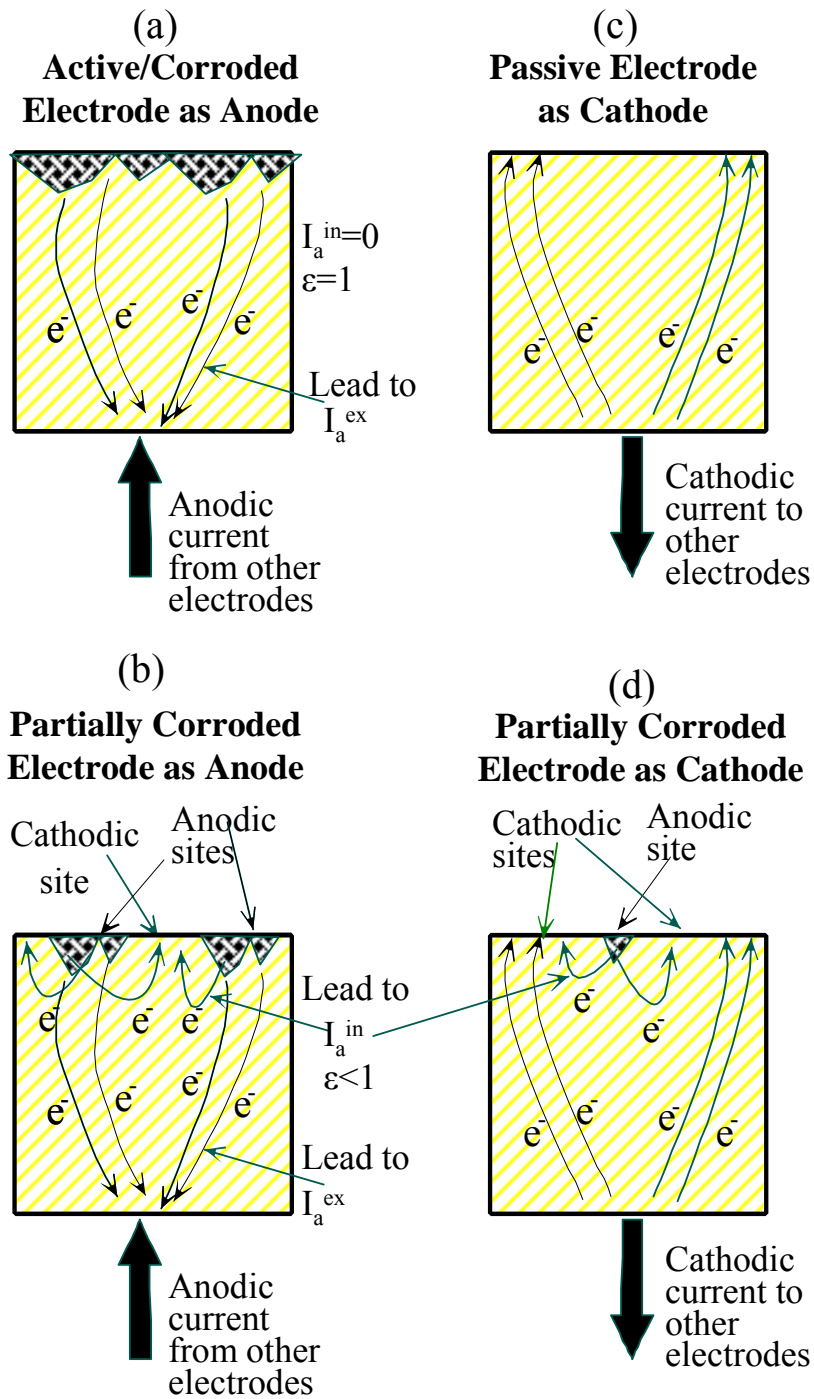


Figure 28. Flow of electrons on (a) a totally corroded active electrode as anode, (b) a partially corroded electrode as anode, (c) a passive electrode as cathode, and (d) a partially corroded electrode as cathode in a CMAS probe. Source: Ref. 89.

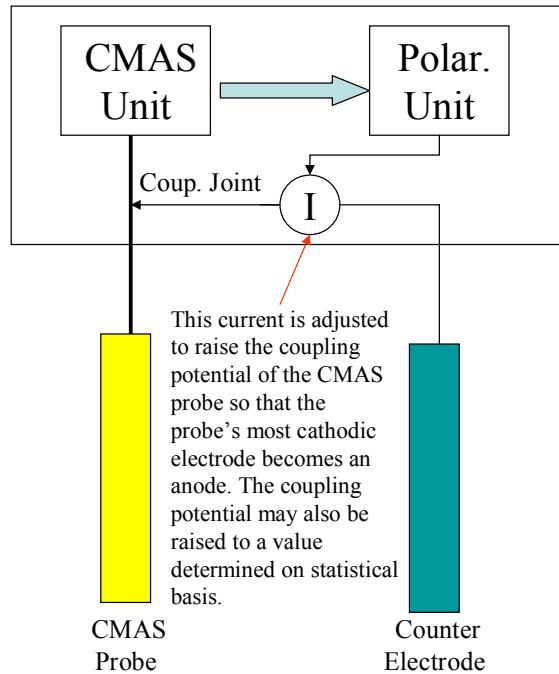


Figure 29. An improved CMAS instrument system that reduces or eliminates the effect of internal electrons on the most anodic electrode of a CMAS probe. Source: Ref. 89.

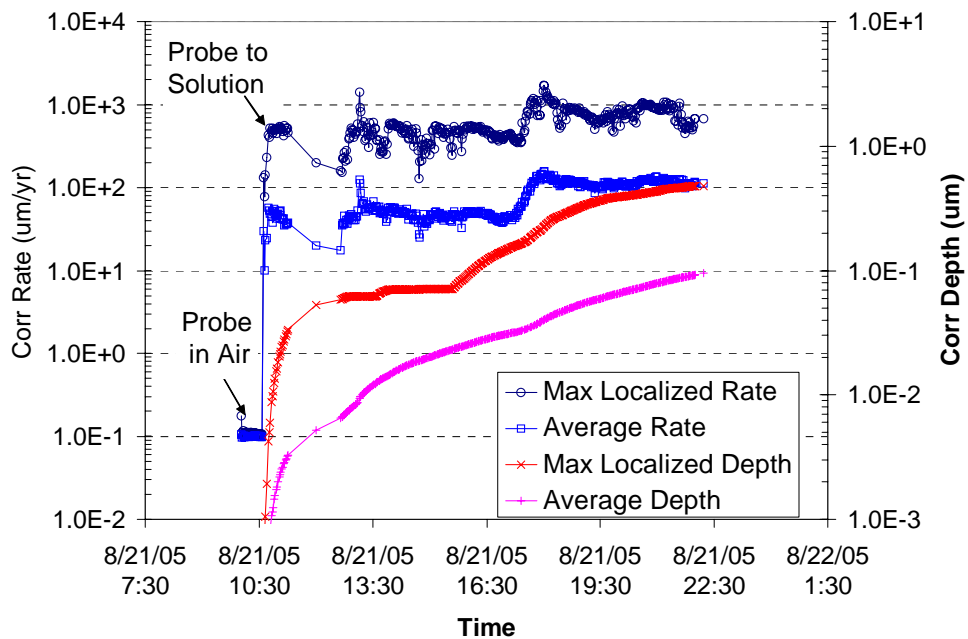


Figure 30. Maximum localized corrosion rate, average corrosion rate, maximum localized corrosion penetration depth, and average corrosion penetration depth measured from a Type 3003 aluminum CMAS probe in simulated seawater. Source: Ref. 93.